



**HAL**  
open science

## What induced the exceptional 2005 convection event in the northwestern Mediterranean basin? Answers from a modeling study.

Marine Herrmann, Jonathan Beuvier, Florence Sevault, Samuel Somot

### ► To cite this version:

Marine Herrmann, Jonathan Beuvier, Florence Sevault, Samuel Somot. What induced the exceptional 2005 convection event in the northwestern Mediterranean basin? Answers from a modeling study.. Journal of Geophysical Research. Oceans, 2010, 115 (C12051), pp.19. 10.1029/2010JC006162 . insu-00562572

**HAL Id: insu-00562572**

**<https://insu.hal.science/insu-00562572>**

Submitted on 3 Feb 2011

**HAL** is a multi-disciplinary open access archive for the deposit and dissemination of scientific research documents, whether they are published or not. The documents may come from teaching and research institutions in France or abroad, or from public or private research centers.

L'archive ouverte pluridisciplinaire **HAL**, est destinée au dépôt et à la diffusion de documents scientifiques de niveau recherche, publiés ou non, émanant des établissements d'enseignement et de recherche français ou étrangers, des laboratoires publics ou privés.

1 **What induced the exceptional 2005 convection event**  
 2 **in the northwestern Mediterranean basin?**  
 3 **Answers from a modeling study**

4 Marine Herrmann,<sup>1</sup> Florence Sevault,<sup>1</sup> Jonathan Beuvier,<sup>1,2</sup> and Samuel Somot<sup>1</sup>

5 Received 1 February 2010; revised 7 October 2010; accepted 15 October 2010; published XX Month 2010.

6 [1] Open-sea convection occurring in the northwestern Mediterranean basin (NWMED) is  
 7 at the origin of the formation of Western Mediterranean Deep Water (WMDW), one of  
 8 the main Mediterranean water masses. During winter 2004–2005, a spectacular convection  
 9 event occurred, observed by several experimental oceanographers. It was associated  
 10 with an exceptionally large convection area and unusually warm and salty WMDW.  
 11 Explanations were proposed tentatively, relating the unusual characteristics of this event  
 12 to the Eastern Mediterranean Transient (EMT) or to the atmospheric conditions during  
 13 winter 2004–2005 in the NWMED. They could, however, not be supported until now.  
 14 Here we used numerical modeling to understand what drove this convection event.  
 15 The control simulation performed for the period 1961–2006 reproduces correctly the  
 16 long-term evolution of the Mediterranean Sea circulation, the EMT, and the NWMED  
 17 convection event of 2004–2005. Sensitivity simulations are then performed to assess  
 18 the respective contributions of atmospheric and oceanic conditions to this event. The  
 19 weakness of the winter buoyancy loss since 1988 in the NWMED prevented strong  
 20 convection to occur during the 1990s, enabling heat and salt contents to increase in this  
 21 region. This resulted in the change of WMDW characteristics observed in 2005. The  
 22 strong buoyancy loss of winter 2004–2005 was responsible for the intensity of the  
 23 convection observed this winter in terms of depth and volume of newly formed WMDW.  
 24 The EMT did not fundamentally modify the convection process but potentially doubled  
 25 this volume by inducing a deepening of the heat and salt maximum that weakened the  
 26 preconvective stratification.

27 **Citation:** Herrmann, M., F. Sevault, J. Beuvier, and S. Somot (2010), What induced the exceptional 2005 convection event in  
 28 the northwestern Mediterranean basin? Answers from a modeling study, *J. Geophys. Res.*, 115, XXXXXX,  
 29 doi:10.1029/2010JC006162.

30 **1. Introduction**

31 [2] Open-sea deep convection takes place in a few regions  
 32 of the world, among which the northwestern Mediterranean  
 33 basin (NWMED) [Marshall and Schott, 1999]. In this region,  
 34 strong winter surface buoyancy loss associated with northern  
 35 wind events (Mistral, Tramontane) induce deep convection  
 36 events, at the origin of the formation of Western Mediter-  
 37 ranean Deep Water (WMDW). During winter 2004–2005, an  
 38 exceptionally strong convection event was observed by  
 39 several experimental oceanographers [López-Jurado *et al.*,  
 40 2005; Salat *et al.*, 2006; Schröder *et al.*, 2006; Font *et al.*,  
 41 2007; Schroeder *et al.*, 2008; Smith *et al.*, 2008]: convection  
 42 reached the bottom and covered an area much larger than  
 43 usually, and WMDW formed this winter was significantly  
 44 saltier and warmer than the values reported in the literature  
 45 (Table 1). Two major explanations for the exceptional

characteristics of this convection event (intensity and 46  
 WMDW characteristics) were proposed by those authors. 47

[3] First, winter 2004–2005 was one of the coldest and 48  
 driest winters of the last 40 years [López-Jurado *et al.*, 49  
 2005; Font *et al.*, 2007], thus associated with strong sur- 50  
 face heat, water and buoyancy losses. The formation of 51  
 dense water at the surface being triggered by the buoyancy 52  
 loss, those atmospheric conditions certainly played a role in 53  
 the intensity of the deep convection event. Moreover, the 54  
 strong water loss must have induced an increase of the 55  
 surface salinity which could partly explain the larger salinity 56  
 of WMDW formed this year. 57

[4] Second, López-Jurado *et al.* [2005] suggested that the 58  
 unusual characteristics of the 2005 convection event could 59  
 be due to an alteration of the water masses advected into the 60  
 convection area. Millot [2005] also proposed that some 61  
 observed changes in the Western Mediterranean Deep Water 62  
 masses could be due to the presence of modified eastern 63  
 waters brought to the Western basin after the Eastern 64  
 Mediterranean Transient (EMT, corresponding to the shift 65  
 of production of Eastern Mediterranean Deep Water from 66  
 the Adriatic to the Aegean subbasins at the beginning of the 67

<sup>1</sup>CNRM-GAME, Météo-France/CNRS, Toulouse, France.

<sup>2</sup>ENSTA-ParisTech/UME, Palaiseau, France.

tl.1 **Table 1.** Observed Characteristics of the Old WMDW (Formed Before 2005) and New WMDW (Formed in 2005)<sup>a</sup>

tl.2	Authors	Old DW			New DW		
		$T_{DW}$ (°C)	$S_{DW}$	$\rho_{DW}$ (kg m <sup>-3</sup> )	$T_{DW}$ (°C)	$S_{DW}$	$\rho_{DW}$ (kg m <sup>-3</sup> )
tl.4	<i>Mertens and Schott</i> [1998]	12.75–12.92	38.41–38.46	29.09–29.10			
tl.5	<i>López-Jurado et al.</i> [2005]	12.83–12.85	38.44–38.46		12.88	38.48–38.49	
tl.6	<i>Schröder et al.</i> [2006]	12.8–12.85	38.44–38.46		12.87–12.90	38.47–38.48	
tl.7	<i>Salat et al.</i> [2006]	12.75–12.82	38.43–38.47	29.115–29.120	12.87–12.90	38.49–38.50	29.130
tl.8	<i>Font et al.</i> [2007]	12.8–12.9	38.43–38.46	29.09–29.10	12.88	38.48	29.117
tl.9	<i>Smith et al.</i> [2008]	12.86	38.46	29.108	12.89	38.48	29.113
tl.10	This study:CTRL, 2005	12.73–12.80	38.423–38.44	>29.10	12.90	38.483	29.116

tl.11 <sup>a</sup>The values obtained in CTRL from the temperature-salinity diagram shown in Figure 7a are also indicated, with old WMDW corresponding to water  
 tl.12 denser than 29.10 kg m<sup>-3</sup> present in LION on 1 December 2004 and new WMDW corresponding to the densest water formed on 10 March 2005.  $T_{DW}$ ,  
 tl.13 temperature;  $S_{DW}$ , salinity;  $\rho_{DW}$ , density.

68 1990s; see *Roether et al.* [2007] for a detailed description of  
 69 the EMT). *Gasparini et al.* [2005] indeed showed that the  
 70 EMT induced an increase of the density of the eastern  
 71 waters flowing westward through the Sicily channel asso-  
 72 ciated with a remarkable injection of heat and salt in  
 73 the deep Tyrrhenian subbasin. Consequently, *López-Jurado*  
 74 *et al.* [2005], *Schröder et al.* [2006] and *Schroeder et al.*  
 75 [2008] suggested that the EMT induced the warming and  
 76 salting of the intermediate and deep layer of the NW MED.  
 77 Being mixed with the rest of the water column when deep  
 78 convection occurs, this layer participates in the composition  
 79 of WMDW. This could thus explain the warming and salting  
 80 of WMDW formed in 2005. Moreover, it could have  
 81 induced a modification of the water column structure, hence  
 82 of the stratification, which could have impacted the exten-  
 83 sion of the deep convection volume.

84 [5] Until now, those explanations were proposed tenta-  
 85 tively, but have not been supported yet. In particular, the  
 86 relative contributions of the atmospheric and oceanic con-  
 87 ditions to the characteristics of the 2005 deep convection  
 88 event still need to be clearly quantified. Observations were  
 89 indeed very useful to characterize this event, but they do not  
 90 provide sufficiently continuous spatial and temporal cover-  
 91 age to answer to those questions. Realistic numerical  
 92 modeling can help to apprehend the 4-D evolution of the sea  
 93 and therefore help to interpret and understand observations.  
 94 To our knowledge, however, no realistic oceanic simulation  
 95 of the NW MED circulation in 2004–2005 has been per-  
 96 formed until now: *Herrmann et al.* [2009] presented a  
 97 simulation that was carried out for the 1998–2007 period,  
 98 but it did not reproduced the change of WMDW char-  
 99 acteristics observed in 2005. In this context, our goal is to  
 100 perform realistic numerical modeling of the NW MED 2005  
 101 convection event but also of the long-term Mediterranean  
 102 circulation before 2004, in order to understand precisely  
 103 what triggered this event, and to quantify the contribution of  
 104 the different factors involved.

105 [6] We present the numerical model and the simulations  
 106 in section 2. Results are then presented and discussed in  
 107 section 3. We first examine the long-term evolution of the  
 108 water column until 2004 in the NW MED and the influence  
 109 of the EMT on the NW MED oceanic conditions. We then  
 110 show that the model is able to represent realistically the  
 111 2004–2005 NW MED convection event. Finally, we deter-  
 112 mine which factors were responsible for the exceptional  
 113 characteristics of this event. For that, we assess the influence  
 114 of the oceanic and atmospheric conditions before and during  
 115 winter 2004–2005. Conclusion and future works are pre-

116 sented in section 4. Note that in the following, all the values  
 117 given for temperature and density correspond to potential  
 118 temperature and density.

## 2. Tools and Methods 119

### 2.1. Numerical Model 120

[7] We use the NEMOMED8 model, a Mediterranean 121  
 version of the NEMO numerical ocean model [*Madec*, 2008] 122  
 used and described by *Beuvier et al.* [2010] and *Sevault et al.* 123  
 [2009]. It is an updated version of the model used by *Somot* 124  
*et al.* [2006] and *Herrmann et al.* [2008] to study the 125  
 NW MED deep convection. NEMOMED8 covers the whole 126  
 Mediterranean Sea plus a buffer zone including a part of the 127  
 near Atlantic Ocean (see Figure 1). The horizontal resolution 128  
 is  $1/8^\circ \times 1/8^\circ \cos(\phi)$ , with  $\phi$  the latitude, equivalent to a range 129  
 of 9 to 12 km from the north to the south of the Mediterranean 130  
 domain. The grid is tilted and stretched at the Gibraltar Strait 131  
 in order to better follow the SW-NE axis of the real strait 132  
 and to increase the local resolution up to 6 km. The Gibraltar 133  
 Strait is represented with a two-grid point wide strait. 134  
 NEMOMED8 has 43 vertical Z levels with an inhomogene- 135  
 ous distribution (from Z = 6 m at the surface to Z = 200 m at 136  
 the bottom with 25 levels in the first 1000 m). The bathymetry 137  
 is based on the ETOPO 5' × 5' database [*Smith and Sandwell*, 138  
 1997]. A time step of 20 min is applied. NEMOMED8 has a 139  
 filtered free-surface and partial-cell parametrization. The 140  
 horizontal eddy diffusivity is fixed to 125 m<sup>2</sup> s<sup>-1</sup> for the 141  
 tracers (temperature, salinity) using a Laplacian operator and 142  
 the horizontal viscosity coefficients is fixed to  $-1.0 \cdot 10^{10}$  m<sup>2</sup> 143  
 s<sup>-2</sup> for the dynamics (velocity) using a biharmonic operator. 144  
 A 1.5 turbulent closure scheme is used for the vertical eddy 145  
 diffusivity [*Blanke and Delecluse*, 1993] with an enhance- 146  
 ment of the vertical diffusivity coefficient up to 50 m<sup>2</sup> s<sup>-1</sup> in 147  
 case of unstable stratification. A no-slip lateral boundary 148  
 condition is used and the bottom friction is quadratic. The 149  
 TVD (Total Variance Dissipation) scheme [*Barnier et al.*, 150  
 2006] is used for the tracer advection. NEMOMED8 con- 151  
 serves energy and enstrophy. The solar radiation can pene- 152  
 trate into the ocean surface layers [*Bozec et al.*, 2008]. 153

### 2.2. Forcings 154

#### 2.2.1. Surface Boundary Conditions: Atmospheric Forcing 155

[8] To prescribe air-sea fluxes to the ocean model, we use 157  
 the results of a high-resolution atmospheric data set named 158  
 ARPERA obtained by performing a dynamical downscaling 159  
 of ECMWF fields. Based on the study of the real case of 160

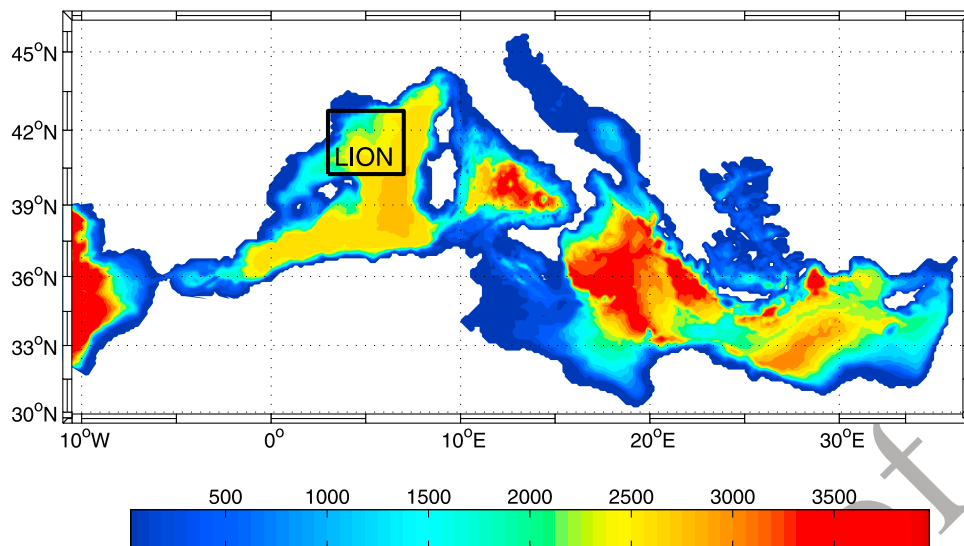


**Figure 1.** Bathymetry of the modeled domain. The black box corresponds to the LION area, from 3°W to 7°W and from 40.25°N to 42.75°N. Unit is meters.

161 winter 1986–1987, *Herrmann and Somot* [2008] showed that  
 162 this data set followed very well the real atmospheric chro-  
 163 nology and was relevant to model realistically deep con-  
 164 vection in the NWMED. The downscaling method was  
 165 described in detail by *Guldberg et al.* [2005]. The principle is  
 166 to use a high-resolution atmospheric model, here ARPEGE-  
 167 Climate [Déqué and Piedelievre, 1995], in which small  
 168 scales can develop freely and large scales are driven by  
 169 ECMWF fields. The synoptic chronology then follows that  
 170 of ECMWF fields while the high-resolution structures of the  
 171 atmospheric flow are created by the model. For the period  
 172 1958–2001, fields of ERA40 reanalysis [Gibson et al., 1997]  
 173 are used to drive ARPEGE-Climat. Between 2002 and  
 174 2006, fields of ECMWF analysis are used, their resolution  
 175 (0.5° ~ 55 km) being downgraded down to ERA40 resolution  
 176 (1.125° ~ 125 km) in order to insure consistency between the  
 177 1958–2001 and 2002–2006 periods.

178 [9] The forcing fields for NEMOMED8 are the momen-  
 179 tum, freshwater and heat fluxes. A relaxation term toward  
 180 ERA40 sea surface temperature (SST) is applied for the heat  
 181 flux. This term actually plays the role of a first-order cou-  
 182 pling between the SST computed by the ocean model and  
 183 the atmospheric heat flux, ensuring the consistency between  
 184 those terms. Following *CLIPPER Project Team* [1999], the  
 185 relaxation coefficient is  $-40 \text{ W m}^{-2} \text{ K}^{-1}$ , equivalent to an  
 186 8 day restoring time scale.

187 [10] The LION area (see Figure 1) is chosen in order to  
 188 cover entirely the region of NWMED deep convection  
 189 reported in the literature [Marshall and Schott, 1999].  
 190 Figure 2 shows the evolution of the mean September–  
 191 November, December–February and September–February  
 192 surface heat, water and buoyancy losses over LION ( $HL$ ,  $WL$   
 193 and  $BL$ ) between winters 1961–1962 and 2005–2006. The  
 194 following formula [Mertens and Schott, 1998] is used for  $BL$ :

$$BL = g \cdot \left( \frac{\alpha \cdot HL}{\rho_0 \cdot C_p} - \beta \cdot SSS \cdot WL \right) = BL_H + BL_W \quad (1)$$

where  $g = 9.81 \text{ m s}^{-2}$  is the gravitational acceleration,  $\rho_0 = 195$   
 1020  $\text{kg m}^{-3}$  is the density reference,  $C_p = 4000 \text{ J kg}^{-1} \text{ K}^{-1}$  is  
 196 the specific heat of water,  $\alpha = 2.10^{-4} \text{ K}^{-1}$  and  $\beta = 7.6.10^{-4}$  are  
 197 the thermal and saline expansion coefficients and  $SSS$  is the  
 198 sea surface salinity. In agreement with what was previously  
 199 observed by *López-Jurado et al.* [2005] using NCEP [Kalnay  
 200 et al., 1996] and by *Font et al.* [2007] using the data of  
 201 the Portbou station from the Catalan Meteorological service,  
 202 the ARPERA data set shows that winter 2004–2005 was the  
 203 coldest and second driest winter of the 1961–2006 period,  
 204 hence the one with the strongest buoyancy loss (highest  
 205 values of  $HL = 265 \text{ W m}^{-2}$  versus  $147 \pm 47 \text{ W m}^{-2}$  in average  
 206 over the 1961–2006 period,  $WL = 4.42 \text{ mm d}^{-1}$  versus  $2.96 \pm$   
 207  $0.79 \text{ mm d}^{-1}$  and  $BL = 1.42 \cdot 10^{-7} \text{ m}^2 \text{ s}^{-3}$  versus  $0.80 \pm 0.24$   
 208  $10^{-7} \text{ m}^2 \text{ s}^{-3}$ ). This was due to the occurrence of several  
 209 intense atmospheric events associated with strong winds and  
 210 to cold and dry air masses, during which  $HL$  and  $WL$  exceeded  
 211  $500 \text{ W m}^{-2}$  and  $10 \text{ mm d}^{-1}$ , respectively. This is shown in  
 212 Figure 3a where we present the evolution of the daily average  
 213 over LION between December 2004 and April 2005 of  $HL$ ,  
 214  $WL$ ,  $BL$  and the wind velocity computed in ARPERA and of  
 215 the wind velocity given by QuikSCAT LEVEL 3 data set  
 216 [Perry, 2001] (available on [http://podaac.jpl.nasa.gov:2031/](http://podaac.jpl.nasa.gov:2031/DATASET_DOCSqscat_l3.html)  
 217 DATASET\_DOCSqscat\_l3.html). Events of strong buoy-  
 218 ancy loss are highlighted in gray in Figure 3. As already  
 219 shown by *Herrmann and Somot* [2008] for winter 1986–  
 220 1987, ARPERA follows very well the real atmospheric  
 221 chronology for winter 2004–2005: the modeled wind velocity  
 222 is correlated with the observed wind velocity obtained from  
 223 QuikSCAT with a correlation factor of 0.970 (significant level  
 224  $>0.999$ ). The wind intensity is also correctly reproduced:  
 225 the mean value over LION between December 2004 and  
 226 March 2005 is equal to  $8.32 \text{ m s}^{-1}$  in ARPERA versus  $9.12 \text{ m}$   
 227  $\text{s}^{-1}$  in QuikSCAT, with a RMSE of  $1.67 \text{ m s}^{-1}$ .  
 228

### 2.2.2. Lateral Boundary Conditions: River, Black Sea and Atlantic Forcings

[11] No salinity damping is used at the surface and a  
 231 freshwater flux due to rivers runoff is explicitly added to  
 232

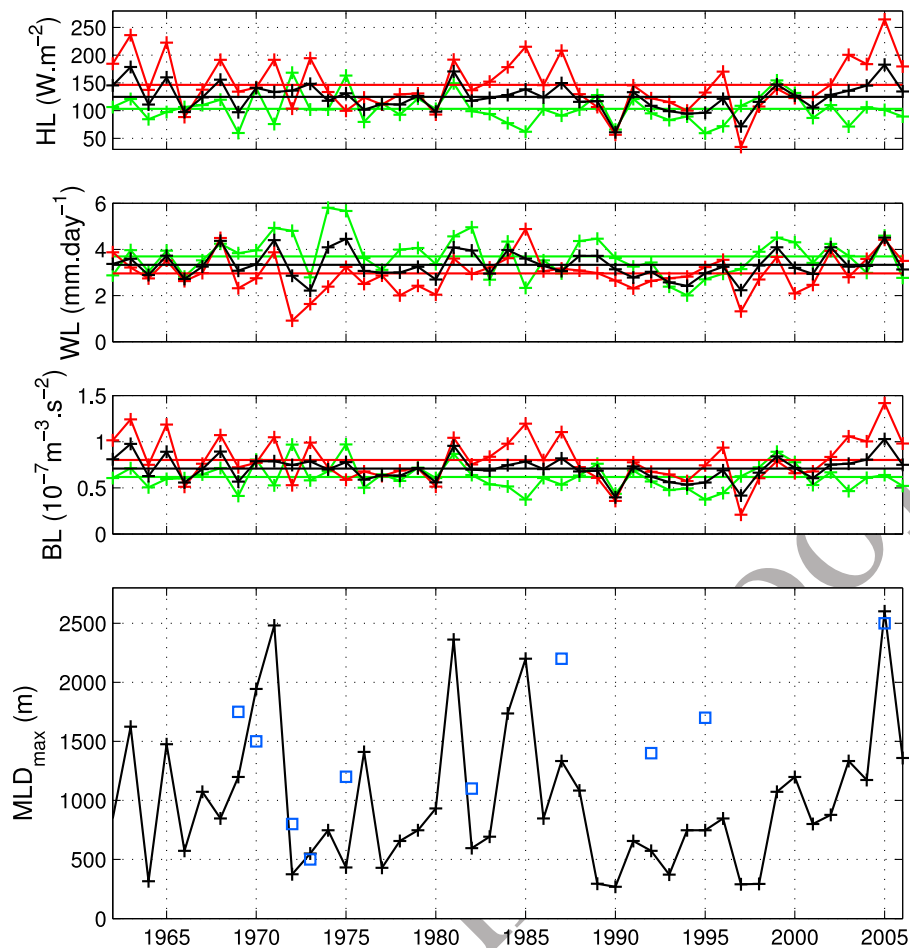


**Figure 2.** Atmospheric forcing and deep convection: time series of the average autumn (September–November, green), winter (December–February, red), and autumn plus winter (September–February, black) surface heat loss ( $HL$ ), water loss ( $WL$ ), and buoyancy loss ( $BL$ ) over LION in ARPERA and of the winter maximum of the spatial maximum of  $MLD$  over LION ( $MLD_{\max}$ ) between winter 1961–1962 and winter 2005–2006. Here 1965 corresponds to winter 1964–1965. For the atmospheric fluxes the horizontal lines indicate the mean values over 1961–2005. Blue squares correspond to observed  $MLD$  values available through several oceanographic cruises and reported by *Mertens and Schott* [1998], *Testor and Gascard* [2006], and *Schröder et al.* [2006].

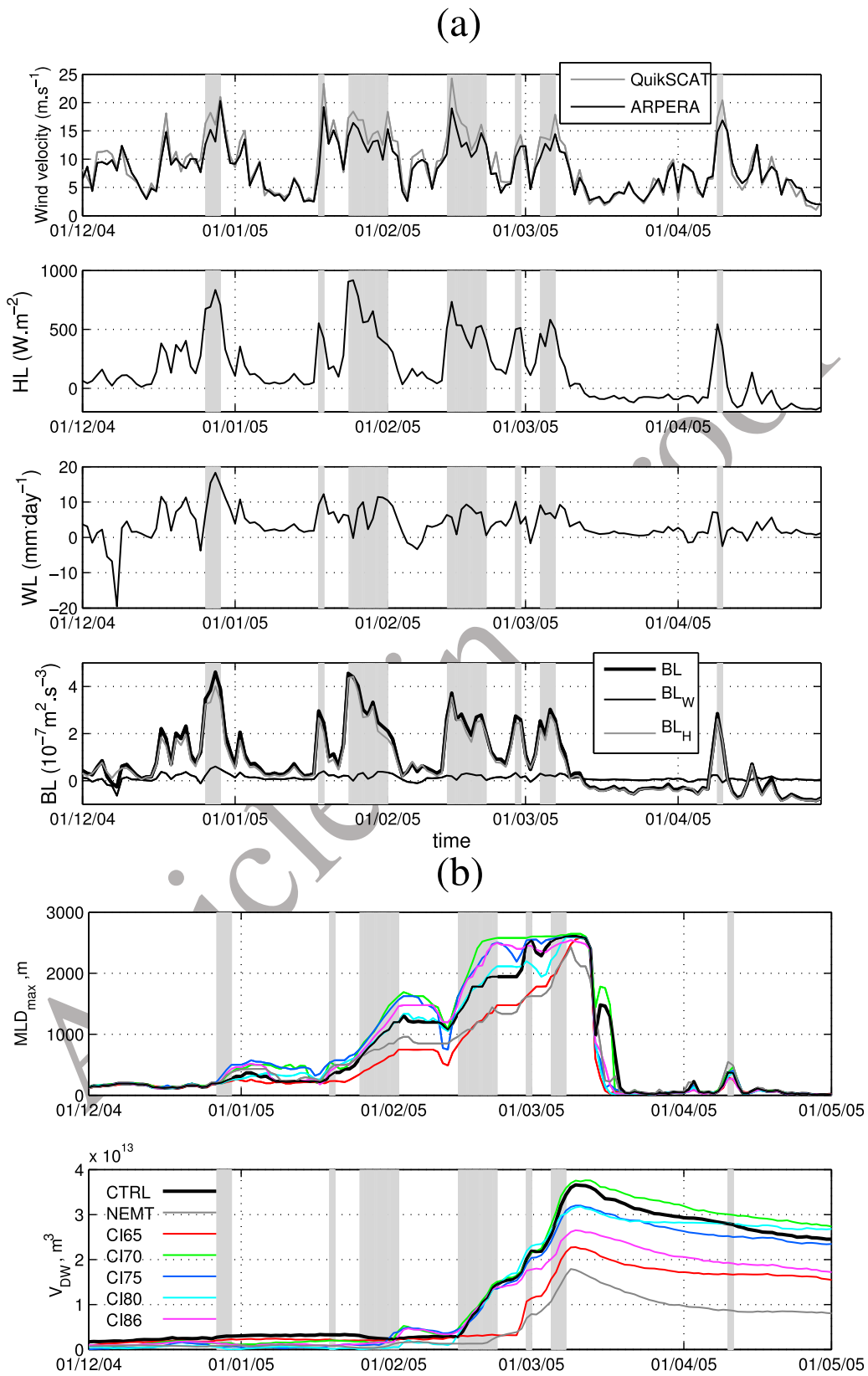
233 complete the surface water budget. Here we use a monthly  
 234 mean climatology (constant over the years) computed from  
 235 the RivDis database [*Vörösmarty et al.*, 1996] for the main  
 236 33 rivers of the Mediterranean Sea catchment basin.

237 [12] The Black Sea, not included in NEMOMED8, is one  
 238 of the major freshwater sources for the Mediterranean Sea.  
 239 The exchanges between the Black Sea and the Aegean  
 240 subbasin consist of a two-layer flow across the Marmara Sea  
 241 and the Dardanelles Strait. We assume that this flow can be  
 242 approximated by a freshwater flux diluting the salinity of the  
 243 mouth grid point. Thus, the Black Sea is considered as a

river for the Aegean. We use a monthly mean climatology 244  
 for this net flux based on the data collected by *Stanev et al.* 245  
 [2000]. 246

[13] The exchanges with the Atlantic Ocean are performed 247  
 through a buffer zone from  $11^{\circ}\text{W}$  to  $7.5^{\circ}\text{W}$ . Temperature 248  
 and salinity in this area are relaxed toward the 3-D T-S 249  
 fields of the seasonal *Reynaud et al.* [1998] climatology by 250  
 means of a Newtonian damping term in the tracer equation 251  
 equal to  $-(X_{\text{model}} - X_{\text{climatology}})/\tau$ . The restoring term is weak 252  
 close to the Gibraltar Strait ( $\tau = 100$  days at  $7.5^{\circ}\text{W}$ ) and 253  
 stronger moving away from it ( $\tau = 3$  days at  $11^{\circ}\text{W}$ ). 254

**Figure 3.** (a) Time series during winter 2004–2005 of the average over LION of the daily wind velocity in ARPERA (black) and QuikSCAT (gray) and of the surface heat, water, and buoyancy losses ( $HL$ ,  $WL$ ,  $BL$ ) in ARPERA. For the buoyancy loss, the thin black (gray) line corresponds to the contribution of the water loss ( $BL_W$ ) (heat loss ( $BL_H$ )), and the thick line corresponds to the total  $BL (= BL_H + BL_W)$ . (b) Time series of the maximum  $MLD$  over LION,  $MLD_{\max}$ , and of the volume of WMDW formed during winter 2004–2005,  $V_{DW}$ , for each simulation performed under the atmospheric forcing of 2004–2005 (CLXX and year 2004–2005 of CTRL and NEMT).



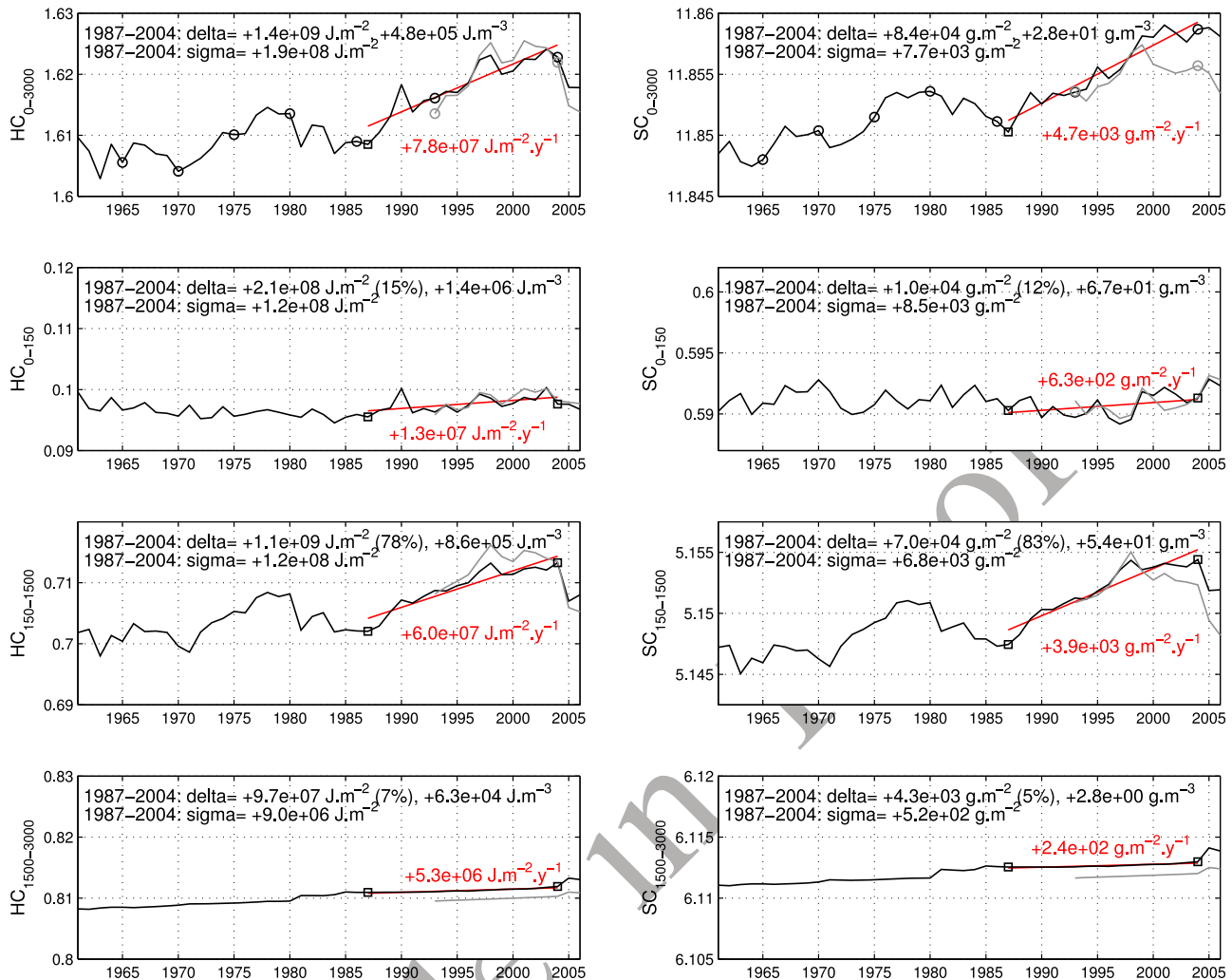


**Figure 4.** Time series of the mean August (left) heat ( $HC$ ,  $10^{11} \text{ J m}^{-2}$ ) and (right) salt ( $SC$ ,  $10^7 \text{ g m}^{-3}$ ) contents of the average water column over LION between 1961 and 2006 in CTRL (black) and between 1993 and 2006 in NEMT (gray) for the whole water column (top line) and the layers 0–150 m (second line), 150–1500 m (third line), and 1500 m to bottom (bottom line). The red line shows the trend between 1987 and 2004 in CTRL, obtained from a linear regression analysis. The value of the trend is indicated in red. Delta indicates the variation of those contents between August 1987 and August 2004 in CTRL, the contribution of each sublayer to the total variation, and the variation of the volumic contents. Sigma is the standard deviation of the time series between 1987 and 2004 in CTRL after the trend has been removed. Circles indicate the years selected to perform the sensitivity simulation CLXX. Squares indicate years 1987 and 2004.

### 255 2.3. Simulations

256 [14] To answer to the scientific questions posed in section 1,  
257 we performed several numerical simulations.

#### 258 2.3.1. Control Simulation CTRL

259 [15] *Beuquier et al.* [2010] performed an oceanic simula-  
260 tion of the Mediterranean circulation for the 1960–2000  
261 period with NEMOMED8, using the forcings presented  
262 above for the surface and lateral boundary conditions (run  
263 NM8-ctrl in their paper). The details of this simulation  
264 (initial conditions, spin-up) are given in their paper. The  
265 initial conditions are given by the MEDATLAS-II clima-  
266 tology [*MEDAR/MEDATLAS Group*, 2002] for the Medi-  
267 terranean part of the model, and by the *Reynaud et al.*  
268 [1998] climatology for the Atlantic buffer zone. A 15 year

269 spin-up was then performed before to launch the simulation  
270 in August 1960. *Beuquier et al.* [2010] showed that the EMT  
271 was realistically reproduced in this simulation: due to an  
272 accumulation of dense water in the Aegean during the 1980s  
273 and beginning of the 1990s, plus a strong buoyancy loss  
274 over the Aegean during winters 1991–1992 and 1992–1993,  
275 very dense water ( $\rho > 29.2 \text{ kg m}^{-3}$ ) filled 75% of the Aegean  
276 in 1993. This water then cascaded through the Cretan Arc  
277 sills into the Ionian and Levantine subbasins and propagated  
278 through the rest of the Eastern basin. They also validated the  
279 evolution over the period 1960–2000 of the heat and salt  
280 contents of the different layers of the Mediterranean Sea,  
281 by comparing them to the interannual values given by *Rixen*  
282 *et al.* [2005].

t2.1 **Table 2.** Simulations Used in This Study: Name of the Simula-  
t2.2 tion, Atmospheric Forcing Used During the Simulation, and Ocea-  
t2.3 nic Conditions at the Beginning of the Simulation

t2.4	Name	Atmospheric Forcing: ARPERA	Initial Oceanic Conditions
t2.5	CTRL	Aug 1960 to Aug 2005	After the initial spin-up: Aug 1960
t2.6			
t2.7	CI65	Aug 2004 to Aug 2005	Aug 1965 of CTRL
t2.8	CI70	Aug 2004 to Aug 2005	Aug 1970 of CTRL
t2.9	CI75	Aug 2004 to Aug 2005	Aug 1975 of CTRL
t2.10	CI80	Aug 2004 to Aug 2005	Aug 1980 of CTRL
t2.11	CI86	Aug 2004 to Aug 2005	Aug 1986 of CTRL
t2.12	AF65	Aug 1965 to Aug 1966	Aug 2004 of CTRL
t2.13	AF70	Aug 1970 to Aug 1971	Aug 2004 of CTRL
t2.14	AF75	Aug 1975 to Aug 1976	Aug 2004 of CTRL
t2.15	AF80	Aug 1980 to Aug 1981	Aug 2004 of CTRL
t2.16	AF86	Aug 1986 to Aug 1987	Aug 2004 of CTRL
t2.17	NEMT	Aug 1993 to Aug 2005	Aug 1980 of CTRL

283 [16] For this study, we extended this simulation until  
284 2006, still using the same forcings (ARPERA for the  
285 atmospheric fluxes, *Vörösmarty et al.* [1996] for the rivers,  
286 *Stanev et al.* [2000] for the Black Sea and *Reynaud et al.*  
287 [1998] for the Atlantic Ocean). In the following, this sim-  
288 ulation is named CTRL.

### 289 2.3.2. Sensitivity Simulations

#### 290 2.3.2.1. Impact of the Oceanic Conditions on the Deep 291 Convection Event: Simulations CIXX

292 [17] To investigate the influence of oceanic conditions on  
293 the convection event, we performed a first group of sensi-  
294 tivity simulations varying the oceanic conditions before the  
295 beginning of the convection event, i.e., in August 2004. For  
296 that, we selected contrasted initial oceanic conditions from  
297 the CTRL simulation: we considered the mean August heat  
298 and salt contents over the whole water column in LION  
299 (Figure 4) and selected five contrasted oceanic conditions  
300 before the beginning of the EMT, i.e., before 1987: 1965,  
301 1970, 1975, 1980 and 1986. The heat and salt contents over  
302 LION,  $HC$  (unit:  $J m^{-2}$ ) and  $SC$  (unit:  $g m^{-2}$ ), are computed  
303 using the following formula:

$$HC = \frac{1}{A_{LION}} \times \iint \int_{LION} c_p \rho(x, y, z) T(x, y, z) dx dy dz$$

$$SC = \frac{1}{A_{LION}} \times \iint \int_{LION} \rho(x, y, z) S(x, y, z) dx dy dz \quad (2)$$

304 where  $A_{LION} = 9.40 \cdot 10^{10} m^2$  is the surface of the LION area.  
305 The division by  $A_{LION}$  is done in order to obtain an average  
306 surfacic value for a column of  $1 m^2$  of the LION area, so that  
307 we will be able to compare it with the surface and lateral  
308 fluxes in the following. Five simulations were then launched  
309 in August 2004 using those oceanic conditions as initial  
310 conditions, and the same atmospheric conditions as CTRL,  
311 i.e., ARPERA from August 2004. Those simulations are  
312 named CI65, CI70, CI75, CI80 and CI86 in the following.

#### 313 2.3.2.2. Impact of the Atmospheric Conditions on the 314 Deep Convection Event: Simulations AFXX

315 [18] We performed a second group of sensitivity simula-  
316 tions in order to investigate the influence of atmospheric  
317 forcing during the convection event: we ran five simulations  
318 from August to May taking the same initial oceanic condi-  
319 tions, those of August 2004 of CTRL, but varying the  
320 atmospheric forcing. For that we took the atmospheric

forcing of August 1965 to May 1966, August 1970 to May 321  
1971, August 1975 to May 1976, August 1980 to May 1981 322  
and August 1986 to May 1987 from ARPERA. Those 323  
simulations are named AF65, AF70, AF75, AF80 and AF86 324  
in the following. 325

#### 2.3.2.3. Impact of the EMT on the 2005 Convection

##### Event: Simulation NEMT

[19] One of our main objectives is to determine the impact 328  
of the EMT on the NW MED convection event of 2004– 329  
2005. For that, we performed an additional simulation 330  
beginning in August 1993, i.e., just after the EMT, but with 331  
the oceanic conditions of August 1980, which are close to 332  
August 1993 from the point of view of the heat and salt 333  
contents (see Figure 4). This simulation is called NEMT. It 334  
cannot contain the EMT signal that occurred between 1987 335  
and 1993, but it is influenced by the same long-term (1993– 336  
2004) external forcings as CTRL (surface, hydrologic and 337  
lateral boundary conditions). The differences between 338  
NEMT and CTRL can therefore be mainly attributed to the 339  
impact of the EMT. 340

[20] The characteristics of the simulations performed for 341  
this study are summarized in the first three columns of Table 342  
2: name of the simulation, atmospheric forcing and initial 343  
oceanic conditions. 344

## 3. Results

### 3.1. Characteristics of the NW MED Water Column Between 1960 and 2004: Long-Term Evolution and Influence of the EMT

[21] In this section we examine the factors responsible for 349  
the evolution until autumn 2004 of the oceanic conditions in 350  
the NW MED in terms of heat and salt contents and structure 351  
of the water column. 352

#### 3.1.1. Evolution of the Heat and Salt Contents

[22] *Schroeder et al.* [2010] observed that the salt and heat 354  
contents of the water column in the NW MED were anom- 355  
alously high in 2004. This is reproduced in the CTRL 356  
simulation: between August 1987 and August 1998, the heat 357  
and salt contents in LION increase regularly, then remain 358  
relatively stable until August 2004 (Figure 4). As a result, 359  
between 2000 and 2004, these contents are the highest of the 360  
whole 1960–2005 period. Between 1987 and 2004, the 361  
variation of heat and salt contents are equal to  $1.4 \cdot 10^9 J m^{-2}$  362  
and  $8.4 \cdot 10^4 g m^{-2}$ , respectively. Performing a linear 363  
regression analysis, we compute trends of those contents 364  
between 1987 and 2004 of  $+7.8 \cdot 10^7 J m^{-2} yr^{-1}$  and  $+4.7 \cdot 10^3 g m^{-2} yr^{-1}$ , 365  
respectively. The standard deviations of the 366  
detrended signals are equal to  $1.9 \cdot 10^8 J m^{-2}$  and  $7.7 \cdot 10^3 g m^{-2}$ , 367  
respectively: those values are 1 order smaller than the 368  
values of the variation between 1987 and 2004. The increase 369  
observed during this period is therefore statistically signifi- 370  
cant and not simply due to the interannual variability. 371

[23] *Schroeder et al.* [2008] suggested that these anom- 372  
alously high contents could be partly due to an anomalously 373  
high arrival of heat and salt from the Eastern basin. How- 374  
ever, the regularity of this increase in the model suggests 375  
that it is not the case. Moreover, the evolution of the heat 376  
and salt contents is very similar in NEMT (Figure 4), which, 377  
by construction, does not contain any signal due to the EMT 378  
contrary to CTRL. This shows that this increase of heat and 379  
salt contents, whatever its origin, was not related to the 380

381 EMT. Note that on 1 December 2004, the heat contents are  
382 quasi equal in NEMT and CTRL, but that the salt content is  
383 slightly higher in CTRL. This suggests that the EMT  
384 accentuated the salt content increase, perhaps by increasing  
385 the salt content of the intermediate and deep water masses  
386 originating from the Eastern basin and circulating in the  
387 NW MED. Nevertheless this effect is small compared to the  
388 long-term increase occurring during the 1990s.

389 [24] *Schroeder et al.* [2010] observed that the high heat  
390 and salt contents in 2004 were related to an intermediate  
391 layer warmer and saltier than the average: they showed that  
392 the difference compared to the climatology was the stron-  
393 gest in the 500–1000 m layer. The evolution of the heat and  
394 salt contents in each main layer of the average water column  
395 over LION in CTRL and NEMT is indicated in Figure 4:  
396 surface layer of Atlantic Water (0–150 m), intermediate  
397 layer of Levantine Intermediate Water (LIW, 150–1450 m)  
398 and deep layer of WMDW (1450 m to bottom). The values  
399 obtained for the variation of heat and salt contents between  
400 1987 and 2004 in each layer are indicated for CTRL in  
401 Figure 4, as well as the values of the contribution of each  
402 layer to the total variation, the trend between 1987 and  
403 2004, and the standard deviation of the detrended signal  
404 between 1987 and 2004. In the intermediate and deep layers,  
405 the 1987–2004 variation is 1 order of magnitude larger than  
406 the standard deviation of the detrended signal. The increase  
407 in these layers is therefore significant and not due to the  
408 interannual variability. On the contrary, in the surface layer,  
409 the variation between 1987 and 2004 is of the same order  
410 than the standard deviation of the detrended signal: the  
411 difference between 1987 and 2004 cannot be clearly  
412 attributed to a positive trend, but is rather due to the inter-  
413 annual variability. This can be explained by the fact that  
414 contrary to the deep and intermediate layers, the surface  
415 layer is directly submitted to the strong seasonal variability  
416 of the atmospheric forcing. Finally during the 1990s, the  
417 heat and salt contents significantly increase only in the deep  
418 and intermediate layers. The warming and salting of the  
419 whole water column is mainly due to the warming and  
420 salting of the intermediate layer that represent 78% and  
421 83%, respectively, of the total increase.

422 [25] The evolution between 1961 and 2006 in CTRL of  
423 the yearly maximum of the spatial maximum of the daily  
424 mixed layer depth (MLD) over LION,  $MLD_{max}$ , is pre-  
425 sented in Figure 2 (black line for CTRL). Comparing the  
426 evolution of  $MLD_{max}$  with the evolution of the total heat and  
427 salt contents shows that those contents increase during the  
428 periods of weak convection (1971–1979, 1988–1998) and  
429 decrease or remain approximately constant during the peri-  
430 ods of stronger convection (1961–1970, 1981–1987, 1999–  
431 2006). Indeed, when deep convection occurs, the water  
432 column is mixed, producing WMDW. When convection  
433 ceases after the winter, the salt and heat originally contained  
434 in the warm and salty intermediate layer are exported with  
435 the WMDW in the deep layer then out of the convection  
436 area [*Herrmann et al.*, 2008]. This results in a transfer of  
437 heat and salt from the intermediate layer into the deep layer.  
438 This abrupt removal (input) of heat and salt from the  
439 intermediate layer (into the deep layer) was observed by  
440 *Schroeder et al.* [2010] after the convection event of winter  
441 2004–2005. It is reproduced in CTRL, for example after the  
442 strong convection events of winters 1980–1981 and 2004–

2005, that both occurred after several winters without deep  
convection (Figures 4 and 2). Salt and heat are then pro-  
gressively reintroduced in the intermediate layer when the  
salty and warm LIW originating from the Eastern basin  
[*Millot*, 1999] spreads into the NW MED. If convection does  
not occur during a few years, the heat and salt contents of  
the intermediate layer will therefore increase until warm and  
salty LIW has completely refilled this layer. As will be  
shown in section 3.3.1, the intensity of deep convection  
depends on the winter buoyancy loss: deep convection  
occurs when the winter buoyancy loss is sufficiently strong,  
enabling the initially stratified water column to be mixed to  
great depth. Between 1988 and 2001, the winter buoyancy  
loss was generally lower than the average, explaining that  
convection was weak during this period (Figure 2). Our  
results therefore suggest that the exceptionally high heat and  
salt contents in 2004 were not due to an anomalously high  
arrival of heat and salt induced by the EMT, but to the  
absence of strong convection during the 1990s. This absence  
would have resulted from the weakness of the winter  
atmospheric buoyancy loss during this period and enabled  
the heat and salt to accumulate in the intermediate layer.

[26] Observed values of MLD available thanks to several  
oceanographic campaigns reported by *Mertens and Schott*  
[1998], *Testor and Gascard* [2006] and *Schröder et al.*  
[2006] are also indicated in Figure 2 (blue squares). Com-  
paring the data and the model results suggests that the  
absolute value of the modeled MLD is generally under-  
estimated. Data are, however, too scarce to validate the  
representation of the interannual variability of the MLD,  
which is suggested here to play an important role in the long-  
term evolution of heat and salt content in the Gulf of Lion.  
Nevertheless, this comparison put our conclusions into per-  
spectives, reminding that they are obtained thanks to a given  
model forced by a given atmospheric data set. We analyze  
and interpret the results of this model, which is not the reality  
but a tentative to represent it as well as possible using the  
state of the art of the models used to simulate the long-term  
Mediterranean oceanic circulation. It would be necessary to  
perform a group of other simulations using other ocean  
models and other atmospheric forcing in order to enforce the  
robustness of our conclusions or to propose alternative  
explanations. Note, however, that other studies [*Sannino*  
*et al.*, 2009] also suggest that due to weak winter surface  
buoyancy flux, the 1990s was a period of weak convection.  
**3.1.2. Impact of the EMT on the Structure of the Water  
Column**

[27] Analyzing hydrographic data, *Gasparini et al.* [2005]  
showed that in the Sicily channel and in the Tyrrhenian  
subbasin, the EMT resulted in a deepening between 1992  
and 2003 of the heat and salt originating from the Eastern  
Basin. As a result the saltier and warmer waters progres-  
sively extended their influence in depth until 1500 m (see  
Figure 14 of *Gasparini et al.* [2005]). Deep water of eastern  
origin then flows into the NW MED [*Millot*, 1999], we can  
therefore expect from those observations in the Tyrrhenian  
that the EMT induced the deepening of the salty and warm  
intermediate layer in the NW MED. Indeed, the heat and salt  
increase extended deeper in CTRL (until 1500 m; Figure 5),  
in agreement with the observations, than in NEMT where it  
mainly occurred in the “classical” intermediate layer (200–  
1000 m). Our modeling study therefore shows an effect of

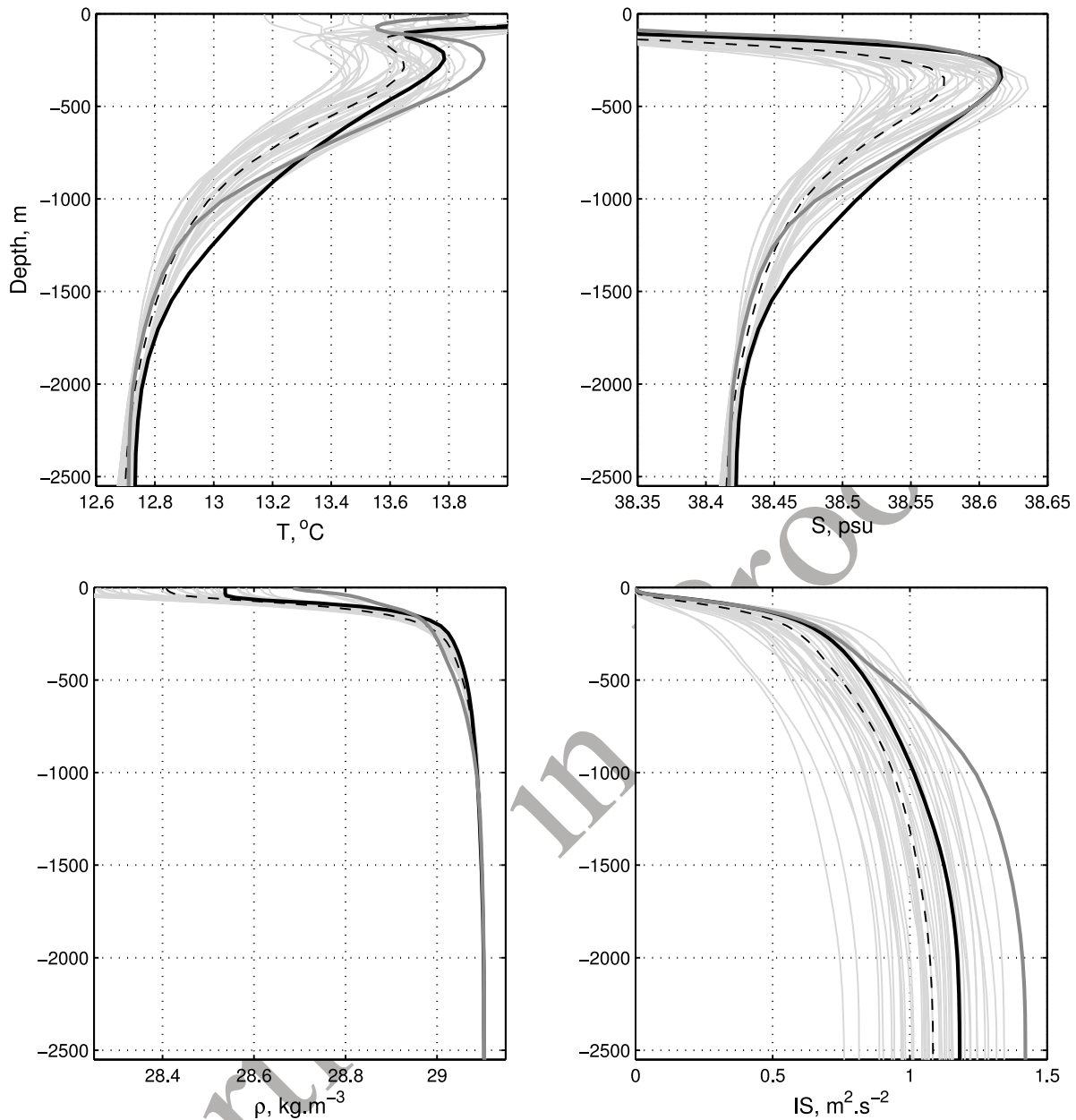


**Figure 5.** Average temperature, salinity, density, and stratification profiles in December over LION. Light gray lines are 1961–2000 for CTRL. Dashed line is average profile over 1961–2000. Black line is 2004 for CTRL. Dark gray line is 2004 for NEMT.

505 the EMT on the structure of the NWMED water column in  
 506 agreement with the observations made by *Gasparini et al.*  
 507 [2005] and *Schroeder et al.* [2010]: the EMT induced a  
 508 deepening of the heat and salt maximum in the NWMED.  
 509 [28] *Gasparini et al.* [2005] showed that this deepening  
 510 was associated with an increase of the density of the warm  
 511 and salty eastern waters flowing in the intermediate and  
 512 deep layers of the Western basin. This increase of the  
 513 density in the intermediate layer is reproduced by the model,  
 514 as can be seen when comparing the CTRL and NEMT  
 515 density profiles (Figure 5). The vertical density gradient  
 516 in these layers consequently decreased. To investigate  
 517 the effect of this modification of the density profile on the  
 518 stratification of the NWMED water column, we compute the

total buoyancy flux required to mix an initially stratified 519  
 water column down to the depth  $z$ ,  $IS(z)$ , using the formula 520  
 used by *Herrmann et al.* [2008]: 521

$$IS(z) = \int_0^z N^2(h) \cdot h \cdot dh = \int_0^z \frac{-g}{\rho} \frac{\partial \rho}{\partial h} \cdot h \cdot dh \quad (3)$$

where  $N$  ( $s^{-1}$ ) is the initial Brunt-Väisälä frequency.  $IS$  522  
 represents an index of the stratification of the water column. 523  
 The stratification profiles on December 2004 over LION are 524  
 shown in Figure 5 for CTRL and NEMT. The stratification 525  
 in NEMT is among the strongest of the whole 1961–2004 526  
 period, whereas the stratification in CTRL is only slightly 527  
 above the average. This shows that the EMT induced a 528

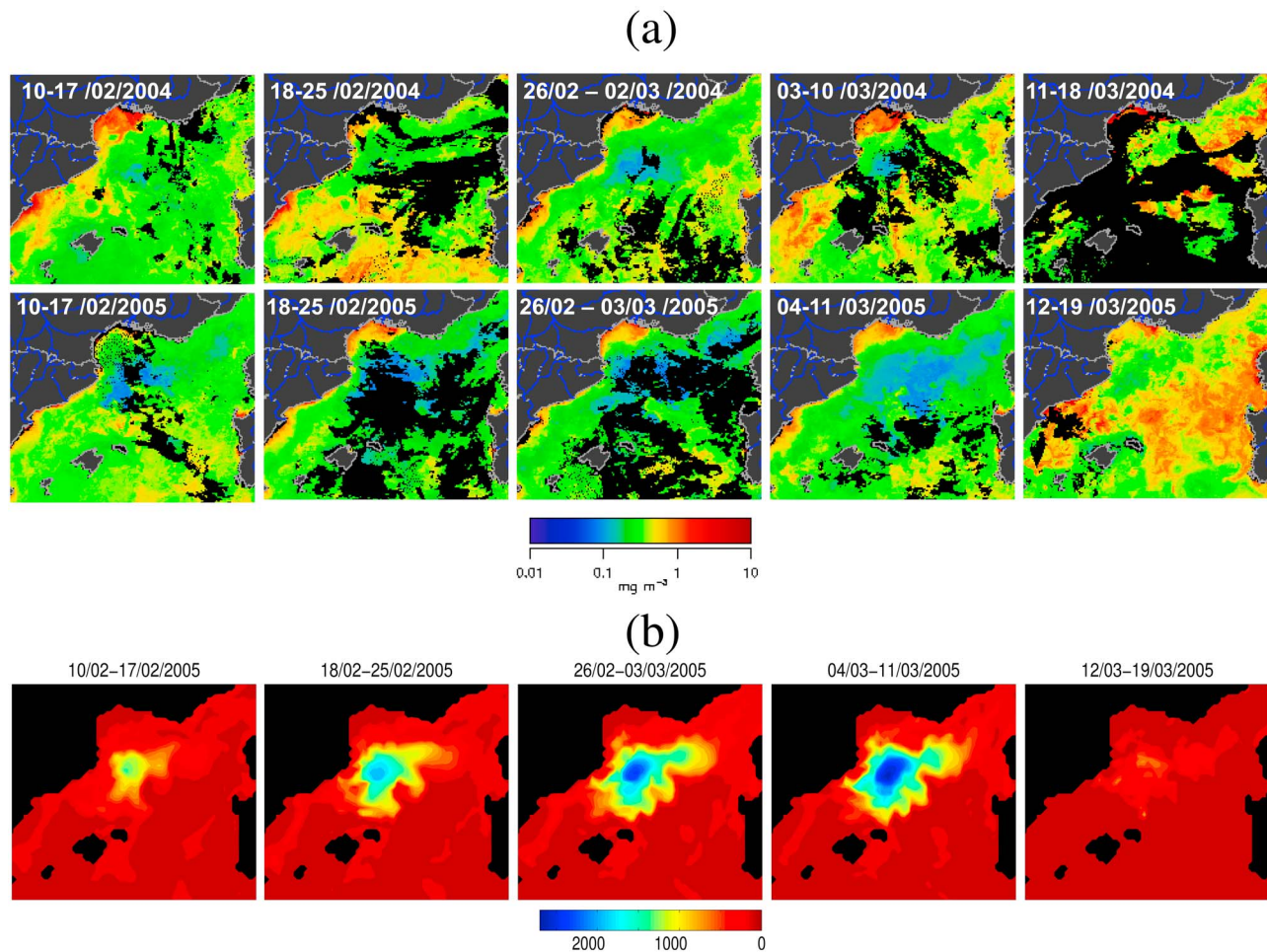


**Figure 6.** (a) Weekly averaged surface chlorophyll concentration observed by MODIS in the NWMED during the winter convection period (mid-February/mid-March) in (top) 2004 and (bottom) 2005 (unit is  $\text{mg m}^{-3}$ ). (b) Maps of the MLD averaged over the same periods in CTRL (unit is meters).

529 weakening of the NWMED stratification compared with  
 530 what would have been the case without the EMT. This  
 531 is due to the fact that  $IS(z)$  being proportional to  $\int z \times \frac{\partial \rho}{\partial z}$ ,  
 532 a decrease of the vertical density gradient in the intermediate  
 533 and deep layer results in a decrease of  $IS$ .

### 534 3.2. Modeling of the 2005 NWMED Convection Event: 535 Validation of the CTRL Simulation

536 [29] All the information concerning the 2004–2005 con-  
 537 vection event available to us was gathered in order to vali-  
 538 date the modeling of this event in CTRL. First, in situ  
 539 observations available in the literature cited in section 1  
 540 provide information about the hydrologic characteristics  
 541 and the structure of the water column in the WMED and  
 542 about the characteristics of the WMDW. Second, satellite  
 543 ocean color data provide information about the temporal and  
 544 spatial evolution of the convection process.

#### 545 3.2.1. Temporal and Spatial Characteristics of the 2005 546 Convection Event

547 [30] The deepest value of  $MLD_{\max}$  between 1961 and  
 548 2006 in CTRL is obtained for 2004–2005 (2601 m), one of  
 549 the four winters of the whole period during which the  
 550 convection reaches the bottom ( $MLD > 2000$  m) in this

simulation (Figure 2). Convection during winter 2004–2005 551  
 is therefore exceptionally strong in CTRL, in agreement 552  
 with the reported observations. 553

[31] MODIS Ocean color data available on <http://marine.jrc.ec.europa.eu> provide an estimate of the extension of the 554  
 convection area. In this area, strong vertical displacements 555  
 indeed prevent the phytoplankton from remaining at the 556  
 surface. The convection area therefore corresponds to the 557  
 region of low chlorophyll concentration. Figure 6a shows 558  
 the maps of the 8 day average chlorophyll obtained from 559  
 MODIS between 10 February and 18 March 2004 and 2005. 560  
 Comparing the 2004 and 2005 maps shows that the particu- 561  
 larly large extension of the convection area in 2005 is well 562  
 captured by those images. 563  
 564

[32] The extension of the low chlorophyll area is the 565  
 largest between 18 February and 11 March 2005, indicating 566  
 that this period was the period of maximum convection. 567  
 Convection does not seem to occur after 12 March. This is 568  
 in agreement with *Smith et al.* [2008] who reported that the 569  
 water column was strongly mixed in the Catalan sea 570  
 between 7 and 12 March. 571

[33] WMDW is identified in our simulations as the water 572  
 of density larger than  $29.1 \text{ kg m}^{-3}$ , following previous 573

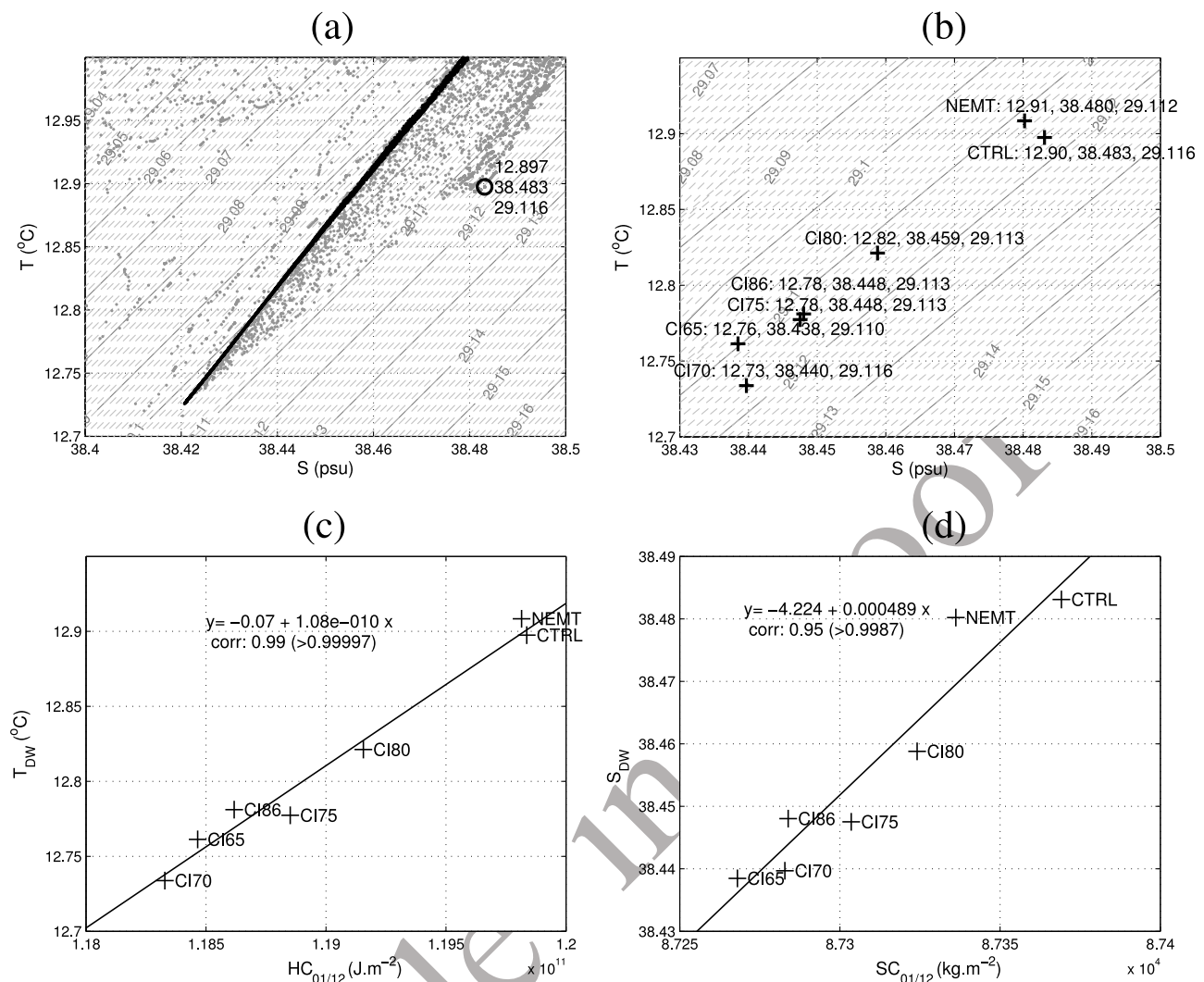


**Figure 7.** WMDW characteristics in simulations performed under the atmospheric forcing of 2004–2005. (a) Temperature-salinity diagram of the water present in LION over the whole column before the convection (1 December 2004, black points) and at the date of maximum convection (10 March 2005, gray points) in CTRL; each point corresponds to a point of the model grid. The characteristics of the densest water present in LION on 10 March 2005 are indicated (black circle). (b) Characteristics ( $T$  (°C),  $S$ ,  $\rho$  (kg m<sup>-3</sup>)) of the densest water present in LION at the date of maximum convection (10 March 2005) for each simulation. (c) Relation between the preconvective heat content over LION,  $HC_{01/12}$ , and the WMDW temperature  $T_{DW}$ . (d) Relation between the preconvective salt content over LION,  $SC_{01/12}$ , and the WMDW salinity  $S_{DW}$ .

574 modeling and observation studies (see, for example, 575 Marshall and Schott [1999] or Herrmann et al. [2008]). 576 Following Herrmann et al. [2008], the volume of newly 577 formed WMDW  $V_{DW}$  is computed each day as the differ- 578 ence between the volume of WMDW present in the 579 NWMED on this day and the minimum of this volume 580 before the convection event, i.e., in autumn 2004 (equal to 581  $13.0 \cdot 10^{13}$  m<sup>3</sup>):  $V_{DW}$  represents an anomaly. The WMDW 582 formation rate  $\tau_{DW}$  is then computed following Castellari 583 et al. [2000] by dividing  $V_{DW}$  by the numbers of seconds 584 in 1 year. Time series between 1 December 2004 and 30 585 April 2005 of the modeled maximum MLD over LION 586  $MLD_{max}$  and of  $V_{DW}$  are shown in Figure 3b (black line for 587 CTRL). The evolution of the convection event follows the 588 atmospheric chronology: each atmospheric event of strong

buoyancy loss induces an abrupt increase of  $MLD_{max}$  and 589  $V_{DW}$ . The mixed layer reaches 1500 m on 17 February, and 590 the bottom is reached between 27 February and 13 March 591 ( $MLD_{max} > 2000$  m), with a small decrease between 1 March 592 and 3 March induced by a decrease of buoyancy loss. This is 593 in agreement with the satellite and in situ observations. The 594 maximum of  $V_{DW}$  is reached on 10 March after the last 595 atmospheric event. It is equal to  $3.66 \cdot 10^{13}$  m<sup>3</sup>, corresponding 596 to a formation rate  $\tau_{DW}$  of 1.16 Sv. This value is consistent 597 with Schroeder et al. [2008], who estimated from in situ 598 observations that the cumulated formation rate for winters 599 2004–2005 and 2005–2006 was approximately equal to 600 2.4 Sv. Then, as soon as the atmospheric BL becomes nega- 601 tive,  $MLD_{max}$  abruptly decreases to zero: restratification of 602 the water column begins, and  $V_{DW}$  starts to decrease. The 603

t3.1 **Table 3.** Preconvection and Convection Characteristics for Each Simulation<sup>a</sup>

t3.2	Name <sup>b</sup>	HC on 1 December ( $10^{11}$ J m <sup>-2</sup> )	SC on 1 December ( $10^4$ kg m <sup>-2</sup> )	IS on 1 December (m <sup>2</sup> s <sup>-2</sup> )	$T_{DW}$ (°C)	$S_{DW}$	$\rho_{DW}$ (kg m <sup>-3</sup> )	$\tau_{DW}$ (Sv)	$MLD_{max}$ (m)	$MLD_{mean}$ (m)
t3.3	CTRL 2004–2005	1.198	8.737	1.02	12.90	38.483	29.116	1.16	2601	943
t3.4	CTRL 1965–1966	1.184	8.727	1.11	no WMDW			0.07	372	94
t3.5	CTRL 1970–1971	1.185	8.729	1.02	12.81	38.451	29.110	0.42	2398	472
t3.6	CTRL 1975–1976	1.186	8.731	0.90	no WMDW			0.14	1416	264
t3.7	CTRL 1980–1981	1.188	8.733	0.84	12.90	38.479	29.113	0.85	2382	510
t3.8	CTRL 1986–1987	1.188	8.728	1.21	no WMDW			0.06	1333	223
t3.9	CI65	1.185	8.727	1.15	12.76	38.438	29.110	0.72	2584	729
t3.10	CI70	1.183	8.728	0.98	12.73	38.440	29.116	1.19	2645	923
t3.11	CI75	1.189	8.730	1.05	12.78	38.448	29.113	1.02	2604	804
t3.12	CI80	1.192	8.732	1.05	12.82	38.459	29.113	1.01	2593	749
t3.13	CI86	1.186	8.728	1.10	12.78	38.448	29.113	0.84	2543	765
t3.14	AF65	1.198	8.737	1.01	no WMDW			0.06	433	118
t3.15	AF70	1.200	8.737	1.06	13.04	38.513	29.110	0.54	1883	564
t3.16	AF75	1.196	8.737	0.86	no WMDW			0.10	1199	282
t3.17	AF80	1.195	8.738	0.77	12.92	38.488	29.115	1.63	2562	768
t3.18	AF86	1.200	8.736	1.15	no WMDW			0.08	1333	291
t3.19	NEMT 2004–2005	1.198	8.734	1.24	12.91	38.480	29.112	0.57	2429	746

t3.20 <sup>a</sup>Given are average heat and salt contents and stratification index at 1000 m over LION on 1 December (HC, SC, and IS), WMDW characteristics ( $T_{DW}$ ,  
t3.21  $S_{DW}$ , and  $\rho_{DW}$ ), WMDW formation rate ( $\tau_{DW}$ ), winter maximum of the maximum MLD over LION ( $MLD_{max}$ ), and winter maximum of the average MLD  
t3.22 over LION ( $MLD_{mean}$ ). When  $MLD_{max} < 1500$  m the convection is not considered as deep but intermediate. No WMDW is formed.

t3.23 <sup>b</sup>Year is also given for CTRL and NEMT.

604 chronology of the convection event reproduced by the model  
605 is therefore in good agreement with the chronology deduced  
606 from the available observations.

607 [34] The modeled area of convection corresponds to the  
608 area obtained from the ocean color data, as can be seen when  
609 comparing the maps of the 8 day average of the modeled  
610 MLD between 10 February and 18 March shown in Figure 6b  
611 and the corresponding ocean color maps. At each period, the  
612 size and position of the modeled convection area corresponds  
613 to the size and position of the observed low chlorophyll  
614 concentration area. The extension of the convection area is  
615 the largest between 26 February and 11 March, as the  
616 extension of the low chlorophyll concentration area.

### 617 3.2.2. Characteristics of WMDW Formed in 2005

618 [35] Figure 7a shows the temperature–salinity diagram  
619 of the water present in LION before the convection event  
620 (1 December 2004) and when the convection reaches its  
621 maximum (10 March 2005). “Old” WMDW, i.e., WMDW  
622 formed before winter 2004–2005, can be identified on  
623 1 December as the water present in LION and denser than  
624  $29.10$  kg m<sup>-3</sup>: in CTRL, characteristics of old WMDW are  
625  $\sim 12.72$ – $12.80$ °C and  $\sim 34.42$ – $38.44$ . They belong to the  
626 range of the observed characteristics of old WMDW reported  
627 in the literature ( $12.75$ – $92$ °C,  $38.41$ – $47$ ; see Table 1).  
628 WMDW formed during winter 2004–2005 can be identified  
629 as the densest water present on 10 March. Its characteristics  
630 ( $T_{DW} = 12.90$ °C,  $S_{DW} = 38.48$  and  $\rho_{DW} = 29.116$  kg m<sup>-3</sup>) are  
631 in very good agreement with the observed characteristics of  
632 WMDW formed in 2005 ( $12.87$ – $90$ °C,  $38.47$ – $50$ ,  $29.113$ –  
633  $130$  kg m<sup>-3</sup>; see Table 1). The change of temperature and  
634 salinity between old and “new” WMDW is therefore also  
635 correctly reproduced ( $\sim +0.1$ – $0.2$ °C and  $\sim +0.04$ – $0.06$ ).

### 636 3.3. Analysis of the Sensitivity Simulations: Which 637 Factors Were Responsible for the Characteristics 638 of the 2005 Convection Event?

639 [36] Having shown that the CTRL simulation represents  
640 correctly the 2004–2005 convection event, we now analyze  
641 the sensitivity simulations in order to determine the

642 respective contributions of the oceanic and atmospheric  
643 conditions to the characteristics of this event.

### 644 3.3.1. Why Was the 2004–2005 Convection Event 645 Exceptionally Strong?

646 [37] In this section we investigate the factors responsible  
647 for the exceptional intensity of the 2005 convection event in  
648 terms of mixed layer depth and volume of newly formed  
649 WMDW: we examine the influence of the stratification of  
650 the water column at the beginning of the convection, of the  
651 EMT and of the atmospheric conditions during 2004.

### 652 3.3.1.1. Impact of the Oceanic Conditions of 2004–2005 653 and of the EMT on the Convection Intensity

654 [38] To investigate the role played by the oceanic condi-  
655 tions in the intensity of the 2004–2005 convection event, we  
656 examine the simulations where the atmospheric forcing is  
657 the one of year 2004–2005 but where the initial oceanic  
658 conditions vary: CIXX and year 2004–2005 of CTRL and  
659 NEMT. For those simulations, the evolution of the maxi-  
660 mum MLD over LION,  $MLD_{max}$ , and of the volume of  
661 newly formed WMDW,  $V_{DW}$ , is presented in Figure 3b. The  
662 chronology of the convection event is the same for all those  
663 simulations: each event of strong atmospheric buoyancy loss  
664 (highlighted in gray in Figure 3) induces an abrupt deep-  
665 ening of the mixed layer and an increase of  $V_{DW}$ , which then  
666 remain relatively stable. The maximum of the convection  
667 intensity, corresponding to the maximum of  $V_{DW}$ , is reached  
668 for all the simulations on 10 March, just after the last event  
669 of strong buoyancy loss occurring in March. At this time,  
670 the convection reaches the bottom in all the simulations:  
671  $MLD_{max}$  varies between 2430 m for NEMT and 2645 m for  
672 CTRL (Table 3). The MLD then abruptly decreases when  
673 the buoyancy loss becomes positive, after 13 March, and  
674  $V_{DW}$  begins to decrease.

675 [39] First, this shows that the chronology of the convec-  
676 tion in terms of deepening/shallowing of the mixed layer  
677 and increase/decrease of  $V_{DW}$  is driven by the succession of  
678 atmospheric events. For year 2004–2005, this resulted in a  
679 strong bottom convection. Second, although bottom con-  
680 vection occurs in all those simulations, the volume of newly

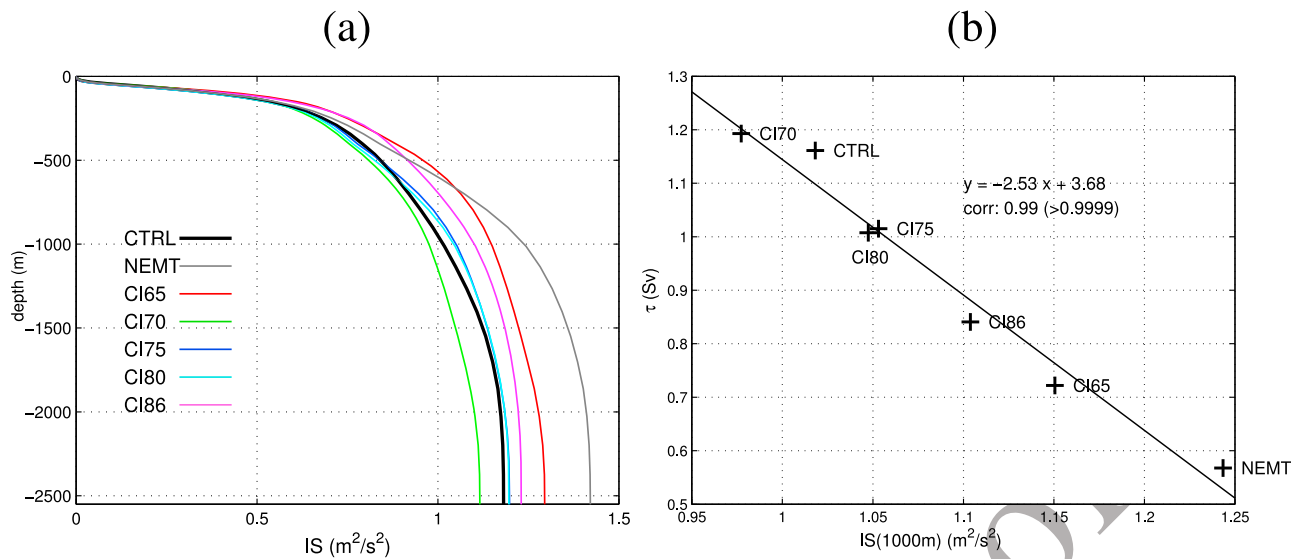


**Figure 8.** (a) For simulations performed under the 2004–2005 atmospheric forcing, average profile over LION of the stratification index on 1 December,  $IS(z)$ . (b) Relation between the average stratification index over LION at 1000 m on 1 December 2004,  $IS(1000m)$ , and the WMDW formation rate,  $\tau_{DW}$ .

681 formed WMDW varies by a factor of 2 between the most  
682 and the less productive simulations ( $\tau_{DW} \sim 0.7$  Sv in CI65  
683 and  $\sim 1.2$  Sv in CI70; Figure 3b and Table 2). This vari-  
684 ability of  $\tau_{DW}$  is actually related to the variability of the  
685 stratification of the water column at the beginning of the  
686 convection: the more stratified the column is, the more  
687 difficult it is to mix it. To show that, we examine the profiles  
688 of  $IS(z)$  before the convection event on 1 December for year  
689 2004 of NEMT, CTRL and CLXX (Figure 8a). The most  
690 stratified water column is obtained in NEMT, and CTRL is  
691 among the simulations with the less stratified water column.  
692 The largest winter maximum of the average  $MLD$  over  
693 LION in 2005 is obtained for CTRL;  $MLD_{mean} = 943$  m,  
694 slightly less than 1000 m (Table 3). We therefore compute  
695 for each simulation the stratification index of the water  
696 column at 1000 m before the convection event on 1 December  
697 2004 (Table 2). Performing a regression analysis between the  
698 WMDW formation rate  $\tau_{DW}$  and  $IS(1000$  m, 1 December  
699 2004), we obtain a strong linear relationship with a corre-  
700 lation factor of 0.99 (SL  $>0.9999$ ) (Figure 8b). For given  
701 atmospheric conditions, here those of winter 2004–2005, the  
702 variability of the intensity of deep convection in terms of  
703 volume of newly formed WMDW is therefore directly related  
704 to the variability of the stratification at the beginning of the  
705 convection, which facilitates or hinders the mixing of the  
706 water column.

707 [40] Comparing the  $IS$  profiles in December 2004 in  
708 NEMT and CTRL, we showed in section 3.1 that the EMT  
709 induced a weakening of the stratification in the NWMD.  
710 As a result, the intensity of deep convection in terms of  
711 WMDW formed is twice stronger in CTRL than in NEMT.  
712 **3.3.1.2. Impact of the Atmospheric Conditions of 2004–**  
713 **2005 on the Convection Intensity**

714 [41] Figure 5 shows the profiles of  $IS(z)$  before the con-  
715 vection event on 1 December for all the years of the CTRL  
716 simulation and for year 2004 of NEMT. The water column  
717 on 1 December 2004 in NEMT is the most stratified of all the

years; however, the convection reaches the bottom. This  
718 suggests that the atmospheric buoyancy loss in 2004–2005  
719 played the most determining role in the intensity of the  
720 convection event: it was so strong that convection could have  
721 reached the bottom even for the most stratified conditions.  
722

[42] To confirm the influence of the atmospheric condi-  
723 tions on the intensity of the 2004–2005 convection event,  
724 we examine the simulations where the initial oceanic condi-  
725 tions are those of August 2004 but where the atmospheric  
726 forcing varies: AFXX and year 2004–2005 of CTRL. For  
727 those simulations, the evolution of the atmospheric buoy-  
728 ancy loss, of  $MLD_{max}$  and of  $V_{DW}$  is presented in Figure 9.  
729 The variability of the convection depth and newly formed  
730 WMDW volume induced by the atmospheric forcing is  
731 much larger than the variability induced by the oceanic  
732 conditions: there are simulations with no convection (AF65,  
733  $MLD_{max} = 433$ m) or intermediate convection ( $1000$  m  $<$   
734  $MLD_{max} < 1500$  m, AF70, AF86) and practically no  
735 WMDW formed ( $\tau_{DW} < 0.1$  Sv), and simulations with  $\tau_{DW}$   
736 varying between 0.5 Sv and 1.6 Sv with deeper convection  
737 (AF75,  $MLD_{max} = 1883$ m) or even bottom convection  
738 ( $MLD_{max} > 2000$  m, AF80, CTRL). This confirms that the  
739 factor predominantly responsible for the intensity of deep  
740 convection in 2004–2005 was the atmospheric forcing rather  
741 than the oceanic conditions: with different initial oceanic  
742 conditions of another autumn bottom convection would  
743 have occurred anyway, whereas with different atmospheric  
744 conditions there could have been no convection, interme-  
745 diate convection or bottom convection.  
746

[43] Which aspect of the atmospheric forcing more pre-  
747 cisely drives the convection? We saw that the succession of  
748 strong buoyancy loss event induces the deepening of the  
749 mixed layer during the winter, corresponding to the violent  
750 mixing phase of deep convection defined by *Marshall and*  
751 *Schott* [1999]. We therefore expect the variability of the  
752 intensity of deep convection to be related to the variability  
753 of the cumulated buoyancy loss over this phase. However,  
754

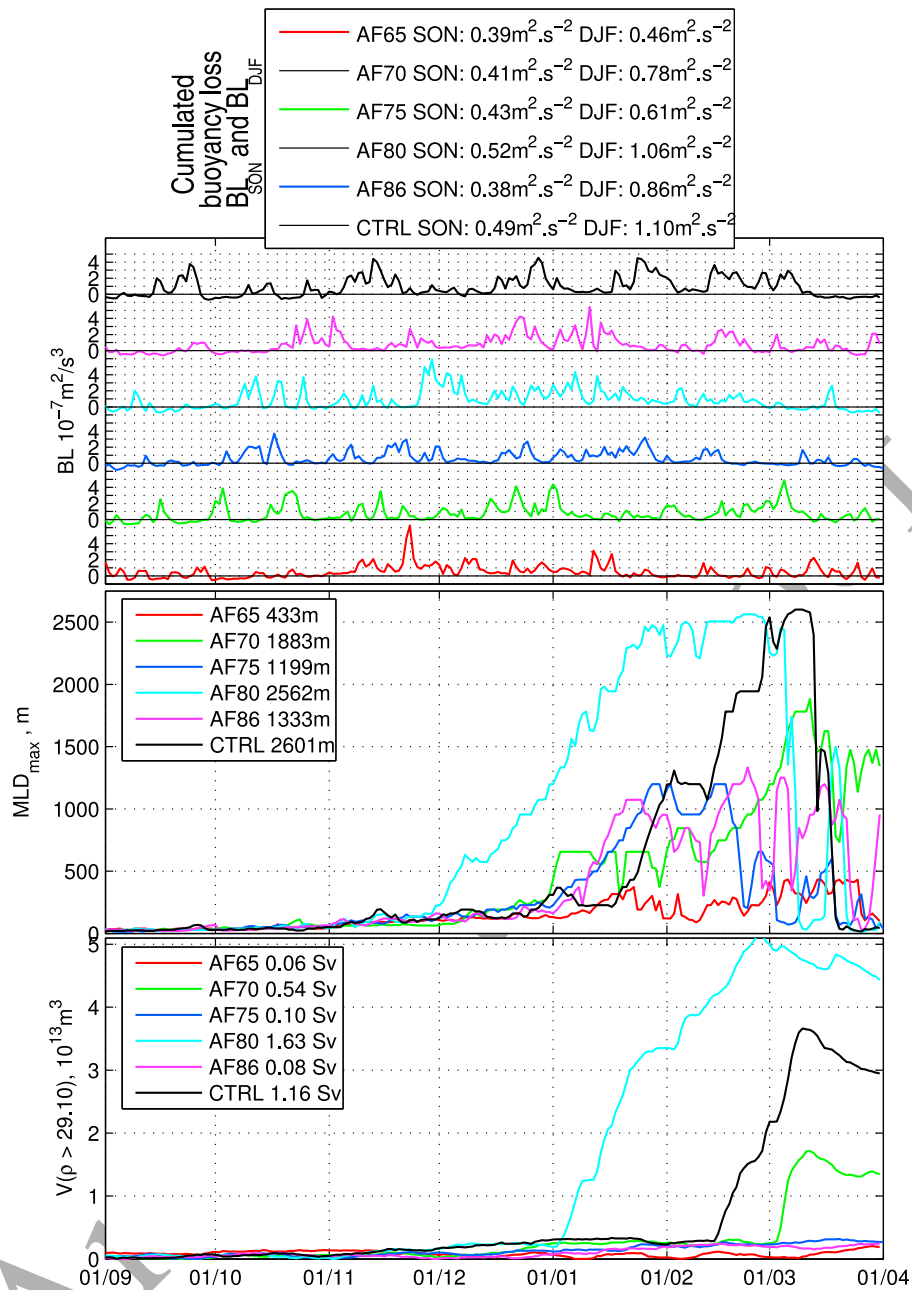


**Figure 9.** For simulations performed with the initial oceanic conditions of August 2004 of CTRL (AFXX and year 2004–2005 of CTRL), time series between September and March of the average buoyancy loss over LION,  $BL$ ; of the maximum MLD over LION,  $MLD_{\max}$ ; and of the volume of newly formed WMDW,  $V_{DW}$ . For each simulation we indicate the values of (top) the buoyancy loss cumulated over September–November and December–February, of (middle) the maximum of  $MLD_{\max}$ , and of (bottom) the WMDW formation rate.

755 the autumn atmospheric buoyancy loss before this phase, i.  
 756 e., during the preconditioning phase [Marshall and Schott,  
 757 1999], certainly also plays an important role: it partici-  
 758 pates to the weakening of the stratification of the water  
 759 column. The times series of the mean atmospheric buoyancy  
 760 loss over LION during September–November, December–  
 761 February, and September–February are presented in Figure 2.  
 762 For simulations performed with the same initial oceanic  
 763 conditions, the values of the cumulated buoyancy loss

during those periods,  $BL_{SON}$ ,  $BL_{DJF}$  and  $BL_{SONDJF}$ , are  
 764 reported in Figure 9 (top). The results suggest that an  
 765 atmospheric buoyancy loss stronger than the average is  
 766 necessary both during the preconditioning and during the  
 767 violent mixing in order to produce deep convection. In  
 768 particular, in CTRL and AF80, i.e., the two simulations  
 769 where convection reaches the bottom, buoyancy losses are  
 770 significantly stronger than the average over 1960–2006  
 771 ( $BL_{SON}$  is equal to 0.49 and 0.52  $\text{m}^2 \text{s}^{-2}$  in CTRL and  
 772

773 AF80, respectively, versus an average value of  $0.48 \text{ m}^2 \text{ s}^{-2}$ ,  
 774 and  $BL_{DJF}$  is equal to 1.10 and  $1.06 \text{ m}^2 \text{ s}^{-2}$  versus  $0.63 \text{ m}^2$   
 775  $\text{s}^{-2}$ ). On the contrary in AF65 and AF75,  $BL_{SON}$  (0.39 and  
 776  $0.43 \text{ m}^2 \text{ s}^{-2}$ , respectively) and  $BL_{DJF}$  (0.46 and  $0.61 \text{ m}^2 \text{ s}^{-2}$ ,  
 777 respectively) are both smaller than the average, and the  
 778 MLD does not exceed 1500 m. However, some situations  
 779 are not so straightforward: AF86 does not produce deep  
 780 convection whereas AF70 does, though their values of  
 781  $BL_{DJF}$  ( $0.86$  and  $0.78 \text{ m}^2 \text{ s}^{-2}$ , respectively) are both larger  
 782 than the average and their values of  $BL_{SON}$  ( $0.38 \text{ m}^2 \text{ s}^{-2}$  and  
 783  $0.41 \text{ m}^2 \text{ s}^{-2}$ , respectively) are both smaller than the average.  
 784 More generally, examining the time series of the atmo-  
 785 spheric buoyancy loss and of the maximum MLD between  
 786 1961 and 2006 in CTRL (Figure 2) shows that it is very  
 787 difficult to find a clear relationship between  $BL$  and  
 788  $MLD_{\max}$ : see for example winters 1969–1970, 1975–1976  
 789 and 1986–1987. It would certainly be necessary to consider  
 790 the influence of other factors like the frequency and dura-  
 791 tion of the atmospheric events. A much larger amount of  
 792 simulations would be necessary to build a relevant indicator  
 793 of atmospheric conditions to which the interannual vari-  
 794 ability of the intensity of deep convection could be related.  
 795 This is, however, beyond the scope of this study, that  
 796 focuses on the 2004–2005 case.

797 [44] Finally, our sensitivity simulations suggest that the  
 798 strong atmospheric buoyancy loss observed both during  
 799 autumn 2004 and winter 2004–2005, i.e., during the pre-  
 800 conditioning and the violent mixing, was the major factor at  
 801 the origin of the intensity of the convection observed this  
 802 year. The particularly weak stratification of the water col-  
 803 umn in December 2004 induced by the EMT would have  
 804 then accentuated the effect of this strong atmospheric con-  
 805 ditions and potentially doubled the volume of WMDW  
 806 formed, but would not have fundamentally modify the  
 807 convection process.

### 808 3.3.2. Why Was the WMDW Formed in 2005

#### 809 Exceptionally Warm and Salty?

810 [45] In this section we examine the contributions of the  
 811 oceanic and atmospheric conditions before and during the  
 812 convection event of 2004–2005 to the characteristics of  
 813 the WMDW formed in 2005.

#### 814 3.3.2.1. Impact of the Oceanic Conditions Before and 815 During the 2004–2005 Convection Event on the WMDW 816 Characteristics

817 [46] To investigate the influence of the initial oceanic  
 818 conditions on the characteristics of the WMDW formed in  
 819 2004–2005, we examine the simulations where the atmo-  
 820 spheric forcing is the one of year 2004–2005 but where the  
 821 initial oceanic conditions vary: CLXX and year 2004–2005 of  
 822 CTRL and NEMT (see section 2.3.2). For those simulations,  
 823 the characteristics of WMDW formed during winter 2004–  
 824 2005, corresponding to the densest water found in LION at  
 825 the date of maximum convection (10 March 2005; see  
 826 section 3.3.1), are indicated in Table 3 and in Figure 7b.  
 827 WMDW produced in the CLXX simulations corresponds to  
 828 old WMDW ( $12.73$ – $12.82^\circ\text{C}$ ,  $38.43$ – $38.46$ ; see Table 1),  
 829 whereas WMDW produced in CTRL but also in NEMT  
 830 corresponds to new WMDW ( $\sim 12.9^\circ\text{C}$ ,  $\sim 38.48$ ; see Table 1).  
 831 When convection reaches the bottom, which is the case in  
 832 all the simulations examined here (Figure 3), WMDW is  
 833 formed by mixing of the whole water column. Therefore, we

834 can expect the temperature and salinity of newly formed  
 835 WMDW to depend on the heat and salt contents of this water  
 836 column just before the convection. To confirm this  
 837 hypothesis, we perform a linear regression analysis between  
 838 the WMDW characteristics and the average heat and salt  
 839 contents over LION on 1 December,  $HC_{01/12}$  and  $SC_{01/12}$   
 840 (Figures 7c and 7d). Values of  $HC_{01/12}$  and  $SC_{01/12}$  are  
 841 reported in Table 3.  $T_{DW}$  and  $S_{DW}$  are linearly related to  
 842  $HC_{01/12}$  and  $SC_{01/12}$ , respectively, with correlation factors  
 843 larger than 0.95 (SL > 0.99). The fact that WMDW produced  
 844 in 2005 corresponds to old WMDW characteristics in the  
 845 CLXX simulations and to new WMDW in CTRL suggests  
 846 that the exceptional atmospheric heat and salt losses that  
 847 occurred during winter 2004–2005 were not responsible for  
 848 the observed change of WMDW characteristics, and that this  
 849 change was rather due to the evolution of the oceanic heat  
 850 and salt contents until 2004.

851 [47] To investigate the contribution of the oceanic lateral  
 852 fluxes of heat and salt during the convection to the char-  
 853 acteristics of the WMDW formed in 2005, we perform heat  
 854 and salt budgets over LION between  $t_{init} = 1$  December  
 855 2004 and  $t \leq t_{fin} = 31$  March 2005 for simulations performed  
 856 under the atmospheric forcing of 2004–2005. During this  
 857 period, the variation of heat content over LION is equal to  
 858 the sum of the cumulated surface and lateral fluxes of heat,  
 859 and the variation of salt content is equal to the cumulated  
 860 lateral flux of salt:

$$\begin{aligned} \Delta_{t_{init}-t} HC &= \int_{t_{init}}^t HF_{lat}(t) dt + \int_{t_{init}}^t HF_{surf}(t) dt \\ \Delta_{t_{init}-t} SC &= \int_{t_{init}}^t SF_{lat}(t) dt \end{aligned} \quad (4)$$

861 [48] Note that surface freshwater flux associated to  
 862 evaporation/precipitation (see section 2.2) does not appear  
 863 in this equation. Indeed, freshwater flux does not modify the  
 864 total salt content over the water column: there is no flux of  
 865 salt through the ocean/atmosphere boundary, neither the  
 866 water that evaporates nor the rainwater contain salt. How-  
 867 ever, surface freshwater flux induces a variation of the  
 868 whole volume, and therefore a concentration/dilution that  
 869 results in a modification of the average salinity. Rigorously,  
 870 we should relate the salinity of DW to the average salinity  
 871 over the water column rather than to the total salt content.  
 872 The following scale analysis shows that this is equivalent.

873 [49] The variation of salinity induced by a change of vol-  
 874 ume  $dV$  due to evaporation/precipitation is equal to  $dS_{WF} =$   
 875  $-\frac{S_{WF} dV}{V}$ . The variation of salinity induced by a variation of  
 876 salt content  $\Delta SC$  is equal to  $dS_{HC} = \frac{\Delta SC}{\rho V}$ . Among winters  
 877 examined in our sensitivity simulations, deep convection  
 878 occurs during winters 1970–1971, 1980–1981 and 2004–  
 879 2005. Between December and February, the net freshwater  
 880 flux  $WF_{DJF}$  and the initial salt content on 1 December  $SC_{01/12}$ ,  
 881 in CTRL over the surface area are equal to  $WF_{DJF} \sim 3.9 \text{ mm}$   
 882  $\text{d}^{-1}$  and  $SC_{01/12} \sim 8.729 \times 10^7 \text{ g m}^{-2}$ , respectively, in 1970–  
 883 1971,  $WF_{DJF} \sim 3.6 \text{ mm d}^{-1}$  and  $SC_{01/12} \sim 8.733 \times 10^7 \text{ g}$   
 884  $\text{m}^{-2}$  in 1980–1981 and  $WF_{DJF} \sim 4.4 \text{ mm d}^{-1}$  and  $SC_{01/12} \sim$   
 885  $8.737 \times 10^7 \text{ g m}^{-2}$  in 2004–2005. Those values provide an  
 886 estimate of the interannual variability of winter freshwater

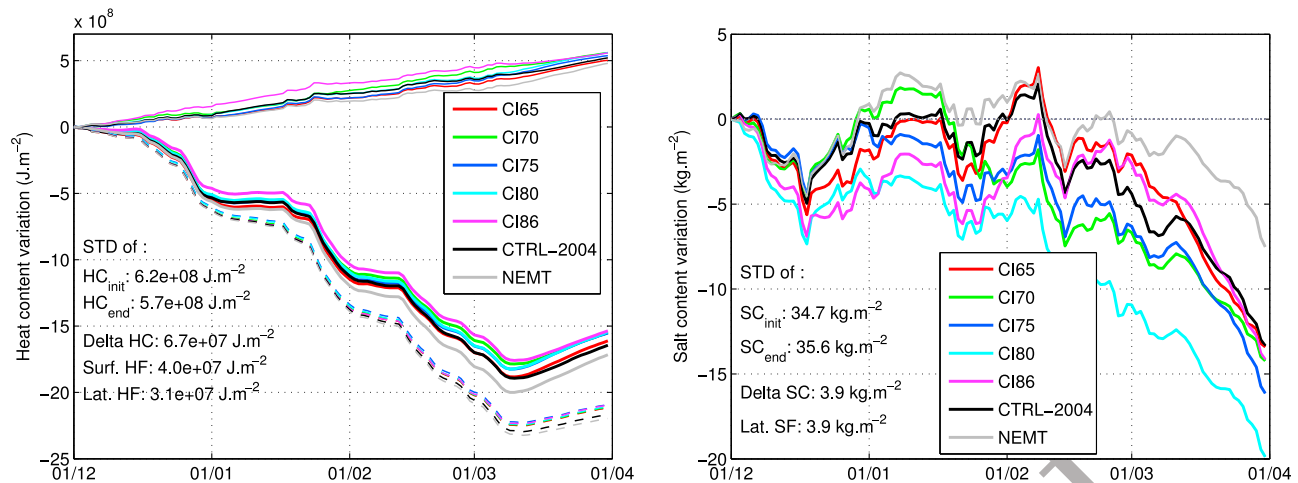


**Figure 10.** (left) Heat and (right) salt budgets over LION between December 2004 and March 2005 in the simulations performed under the atmospheric forcing of 2004–2005. Daily time series of the variation of the total heat and salt contents ( $HC$  and  $SC$ , bold lines), of the cumulated atmospheric heat flux ( $HF_{surf}$ , dashed lines), and of the cumulated lateral heat and salt fluxes ( $HF_{lat}$  and  $SF_{lat}$ , thin lines) since 1 December. Values of the initial contents on 1 December ( $HC_{init}$ ,  $SC_{init}$ ), of the final contents at the date of maximum convection, i.e., 10 March ( $HC_{fin}$ ,  $SC_{fin}$ ), of the variation of the heat content (Delta HC, Delta SC), of the cumulated surface heat flux (Surf. HC), and of the cumulated lateral atmospheric heat and salt fluxes (Lat. HC and Lat. SC) between 1 December and 10 March are indicated in black.

887 flux and initial salt content over years of deep convection. 888 Between winters 1970–1971 or 1980–1981 and winter 889 2004–2005, the difference of freshwater flux is  $\Delta WF_{DJF} =$  890  $[0.5; 0.8] \text{ mm d}^{-1}$  corresponding a difference of volume of 891  $dV = [0.05; 0.08] \text{ m}$  over a period of 100 days (i.e., approxi- 892 mately the length of the convection period, beginning of 893 December to mid-March). The mean height of the water 894 column is  $\sim 2000 \text{ m}$ . The difference of salinity induced by 895 this difference of freshwater flux is therefore  $dS_{WF} \sim 38 \times$  896  $[0.05; 0.08]/2000 = [0.9; 1.5]10^{-3}$ . Between winters 1970– 897 1971 or 1980–1981 and winter 2004–2005, the difference of 898 salt content is  $\Delta SC_{01/12} = [40; 80]10^4 \text{ g m}^{-2}$ . The difference 899 of salinity induced by this difference of salt content is equal 900  $dS_{SC} \sim [40; 80]10^4 / (1029 \times 2000) = [1.9; 3.9]10^{-2}$ .

901 [50] In our model, the variation of salinity induced by the 902 interannual variability of freshwater fluxes during the con- 903 vection period is therefore  $\sim 20$  times smaller than the vari- 904 ation of salinity associated to variability of the initial salt 905 content, hence negligible. This justifies that we could 906 neglect the impact of the freshwater flux on the average 907 salinity and therefore relate the salinity of DW directly to the 908 total salt content, and not only to the average salinity.

909 [51] The evolution of the terms of equation (4) are shown 910 in Figure 10. The evolution of the variation of heat content 911 during the convection event is very similar in each simula- 912 tion, as well as the evolution of the cumulated lateral and 913 surface heat fluxes. As a result, the contribution of those 914 fluxes to the variability of the heat content is 1 order of 915 magnitude smaller than the contribution of the initial heat 916 content: the values of the standard deviation among the si- 917 mulations of the total cumulated lateral and surface heat 918 fluxes between 1 December and 10 March, when the con- 919 vection is the strongest, are equal to  $5 \cdot 10^7$  and  $3 \cdot 10^7 \text{ J m}^{-2}$ , 920 respectively, i.e., approximately 10 to 20 times smaller than

the standard deviation of the initial heat content ( $6 \cdot 10^8 \text{ J m}^{-2}$ ). 921 Similarly, the variability of the lateral salt flux, which 922 evolves similarly in each simulation, is much weaker than 923 the variability of the initial salt content: the standard devi- 924 ation of the total cumulated lateral salt flux is equal to  $3.7 \text{ kg}$  925  $\text{m}^{-2}$ , i.e.,  $\sim 10$  times smaller than the standard deviation of 926 the initial salt content ( $35 \text{ kg m}^{-2}$ ). 927

[52] Our results suggest that for given atmospheric condi- 928 tions, the variability of the characteristics of the newly 929 formed WMDW is mainly related to the variability of the 930 initial heat and salt contents. The lateral oceanic heat and 931 salt fluxes during the convection do not contribute signifi- 932 cantly to the variability of these heat and salt contents, hence 933 to the variability of the WMDW characteristics. 934

### 3.3.2.2. Impact of the Atmospheric Conditions During 935 the 2004–2005 Convection Event on the WMDW 936 Characteristics 937

[53] We showed in section 3.3.1 that the intensity of 938 winter convection in terms of depth is mainly driven by the 939 autumn and winter atmospheric conditions. The deeper the 940 convection is, the larger the amount of WMDW already 941 present in the convection area and mixed with the overlying 942 water is. The relative proportions of WMDW and LIW 943 contributing to the formation of new WMDW are therefore 944 larger and smaller, respectively, when the convection is 945 deeper. For given initial oceanic conditions, the WMDW 946 being less warm and salty than the LIW, the temperature and 947 salinity of the resulting newly formed WMDW will there- 948 fore be smaller for larger depths of convection. This effect 949 can be observed in our modeling study when comparing 950 simulations where initial oceanic conditions are identical 951 and where atmospheric conditions are different but induce 952 deep convection, i.e., year 1970 of CTRL with CI70, year 953 1980 of CTRL with CI80, and AF70, AF80 and year 2004 954

955 of CTRL: for given initial oceanic conditions,  $T_{DW}$  and  $S_{DW}$   
 956 decrease when  $MLD_{max}$  and  $MLD_{mean}$  increase (Table 3). In  
 957 particular, the comparison of AF70, AF80 and year 2004 of  
 958 CTRL shows that if different atmospheric conditions had  
 959 occurred in 2004–2005, e.g., those of winters 1970–1971 or  
 960 1980–1981, deep convection could still have occurred  
 961 ( $MLD_{max} = 1883$  m in AF70, 2562 m in AF80 and 2601 m  
 962 in CTRL) and the change of WMDW could have been even  
 963 more spectacular than the change observed in reality since  
 964 the mixed layer would have been slightly shallower ( $T_{DW}$   
 965 and  $S_{DW}$  are equal to 13.04°C and 38.513 in AF70 and  
 966 12.92°C, 38.488 in AF80 versus 12.90°C, 38.483 in CTRL).  
 967 Another interesting point is that the characteristics of con-  
 968 vection during winter 1980–1981 of CTRL (12.90°C,  
 969 38.479 and 29.113 kg m<sup>-3</sup>) correspond to new character-  
 970 istics: the conjunction of smaller heat and salt contents than  
 971 those of August 2004 (1.188 10<sup>11</sup> J m<sup>-2</sup> and 8.733 10<sup>4</sup> kg  
 972 m<sup>-2</sup> in 1980–1981 versus 1.198 10<sup>11</sup> J m<sup>-2</sup> and 8.737 10<sup>4</sup> kg  
 973 m<sup>-2</sup> in 2004–2005; Figure 4 and Table 3) with smaller  
 974 maximum and mean MLD (2382 m and 510 m versus 2601  
 975 m and 943 m; Table 3) led to the formation of WMDW with  
 976 similar characteristics (12.90°C, 38.479 versus 12.90°C,  
 977 38.483). Finally the atmospheric conditions during the  
 978 convection indirectly influence the characteristics of newly  
 979 formed WMDW by determining the depth of convection.

### 980 3.3.2.3. Impact of the EMT on WMDW Characteristics

981 [54] Finally, the results obtained in sections 3.3.2.2 and  
 982 3.3.2.1 show that the change of temperature and salinity of  
 983 the WMDW formed during winter 2004–2005 compared to  
 984 the WMDW formed before was not due to the atmospheric  
 985 conditions neither to the lateral oceanic advection during  
 986 this winter, but to the initial heat and salt contents of autumn  
 987 2004 over LION, which were exceptionally high. We  
 988 showed in section 3.1 that these high 2004 contents, ob-  
 989 tained both in NEMT and CTRL, were not due to the EMT  
 990 but to the absence of deep convection during the 1990s,  
 991 itself induced by a succession of weak buoyancy loss win-  
 992 ters. Our results therefore show that the EMT was not  
 993 responsible for the change of WMDW characteristics  
 994 observed during the 2005 convection episode, contrary to  
 995 what was suggested by *Schroeder et al.* [2008].

996 [55] Note that this result explains why the simulation used  
 997 by *Herrmann et al.* [2009] in order to study the interannual  
 998 variability of the NW MED convection for the period 1998–  
 999 2007 was not able to reproduce the change of WMDW  
 1000 characteristics observed in 2005. During the 10 years spin-up  
 1001 corresponding to the period 1987–1997, ERA40 fields were  
 1002 indeed used for the atmospheric forcing. Their resolution,  
 1003 ~125 km, is not sufficient to reproduce realistically the  
 1004 Mediterranean circulation and in particular the NW MED  
 1005 deep convection [*Herrmann and Somot*, 2008]. Conse-  
 1006 quently, this simulation could not reproduce correctly the  
 1007 circulation of water masses during this period in the  
 1008 NW MED, and therefore the salting and warming responsible  
 1009 for the change of WMDW characteristics observed in 2005.

## 1010 4. Conclusion

1011 [56] In this paper we focus on the exceptionally strong  
 1012 convection event that occurred in the NW MED during winter  
 1013 2004–2005, associated with newly formed WMDW warmer  
 1014 and saltier than usually. Experimental oceanographers that

observed this event proposed two explanations: the first one 1015  
 relates the exceptional intensity of this convection event, as 1016  
 well as the change of the characteristics of WMDW formed 1017  
 this winter to the atmospheric conditions. The second one 1018  
 relates them to the effect of the EMT on the intermediate 1019  
 layer of the NW MED, hence on the oceanic conditions. We 1020  
 used numerical modeling in order to determine which ele- 1021  
 ment played a role in this event, and how. 1022

[57] We first performed a realistic numerical simulation of 1023  
 the Mediterranean oceanic circulation during the 1960–2006 1024  
 period. The long-term analysis of this simulation was per- 1025  
 formed by *Beuvier et al.* [2010], who validated the long- 1026  
 term evolution of the temperature and salinity in the whole 1027  
 basin, and showed that the model reproduces correctly the 1028  
 EMT. Here we showed that this control simulation is able to 1029  
 reproduce realistically the 2005 NW MED convection event: 1030  
 the temporal and spatial evolution of the convection event as 1031  
 well as the WMDW characteristics were consistent with 1032  
 satellite and in situ observations. 1033

[58] Sensitivity simulations then allowed us to assess the 1034  
 respective contributions of the oceanic and atmospheric 1035  
 conditions to the 2004–2005 convection event. First, we 1036  
 examined the factors that led to the structure of the water 1037  
 column in the NW MED just before the convection. Our model 1038  
 suggests that a succession of winters of weak atmospheric 1039  
 buoyancy loss was responsible for the absence of deep con- 1040  
 vection during the 1990s. This would have enabled the heat 1041  
 and salt to accumulate in the intermediate layer. Conse- 1042  
 quently, the heat and salt contents of autumn 2004 were the 1043  
 highest of the whole 1960–2005 period, in agreement with the 1044  
 observations of *Schroeder et al.* [2010]. According to our 1045  
 model, the EMT did not contribute significantly to this 1046  
 warming and salting of the intermediate layer, but it induced 1047  
 the deepening of the heat and salt maximum in the NW MED. 1048  
 This deepening, already observed by *Gasparini et al.* [2005], 1049  
 was associated with a weakening of the stratification of the 1050  
 water column in autumn 2004 compared to what would have 1051  
 been the case without the EMT. 1052

[59] We then determined which were the key factors that 1053  
 could be responsible for the characteristics of the 2004– 1054  
 2005 convection event. In our model, the abrupt change of 1055  
 WMDW characteristics observed in 2005 predominantly 1056  
 resulted from the high heat and salt contents of autumn 1057  
 2004. It therefore seems that it was not due do the EMT but 1058  
 to the weakness of the winter atmospheric buoyancy loss 1059  
 and deep convection in the NW MED during the 1990s. 1060  
 Moreover, our results suggest that the lateral oceanic heat 1061  
 and salt fluxes during winter 2004–2005 did not play a 1062  
 significant role in the settings of the WMDW characteristics. 1063  
 The atmospheric conditions of 2004–2005, namely the 1064  
 strong autumn and winter atmospheric buoyancy losses, 1065  
 mainly drove the deepening of the mixed layer in our model. 1066  
 They consequently appear to be the major factor responsible 1067  
 for the exceptional intensity of the convection observed this 1068  
 winter in terms of depth and volume of newly formed 1069  
 WMDW. The EMT would have accentuated the effect of the 1070  
 atmospheric forcing by weakening the stratification, hence 1071  
 facilitating the vertical mixing of the water column. This 1072  
 would have not fundamentally change the convection pro- 1073  
 cess and depth but potentially doubled the volume of newly 1074  
 formed WMDW. Finally, our conclusions were obtained 1075  
 using a given ocean model forced by a given atmospheric 1076

1077 data set. It would be necessary to perform other simulations  
1078 using other models and atmospheric forcings in order  
1079 enforce the robustness of our conclusions or to propose  
1080 alternative explanations.

1081 [60] In this study, we focused on winter 2004–2005 and  
1082 on the NWMED in order to understand the mechanisms  
1083 responsible for the spectacular convection that occurred this  
1084 year. WMDW formed in 2005 then propagated into the rest  
1085 of the basin [Schroeder et al., 2008] and a signal apparently  
1086 reached the Gibraltar Strait. García Lafuente et al. [2007]  
1087 indeed observed a decrease of the temperature of the Med-  
1088 iterranean Outflow Water in March 2005 and 2006. They  
1089 attributed it to a remote signature of the strong NWMED  
1090 convection that occurred those winters. Our simulations  
1091 could help to understand how the 2004–2005 convection  
1092 event in the NWMED influenced the circulation in the rest  
1093 of the basin and this motivates further studies. Our next goal  
1094 is to use and perform additional realistic long-term simu-  
1095 lations in order to quantify more generally the contributions  
1096 of the oceanic and atmospheric conditions to the interannual  
1097 variability of the convection characteristics, in the NWMED  
1098 but also in the other regions of deep and intermediate con-  
1099 vection of the Mediterranean Sea (Adriatic, Aegean,  
1100 Levantine subbasins) and study how these local processes  
1101 can interact between each other in particular through the  
1102 thermohaline circulation.

1103 [61] **Acknowledgments.** This study has been sponsored by the  
1104 “Forecast and projection in climate scenario of Mediterranean intense  
1105 events: Uncertainties and Propagation on environment” (MEDUP) project  
1106 of the program Vulnérabilité: Milieux et Climat from the Agence Nationale  
1107 pour la Recherche and by the HyMeX project (Hydrological cycle in  
1108 the Mediterranean experiment ([www.hymex.org](http://www.hymex.org))). We thank C. Millot,  
1109 K. Schroeder, and an anonymous reviewer for their comments and sugges-  
1110 tions that helped to improve the quality of this paper. We also thank  
1111 D. Quoc-Phi, M. Remaud, and A. Verrelle for their work at the very begin-  
1112 ning of this study.

## 1113 References

1114 Barnier, B., et al. (2006), Impact of partial steps and momentum advection  
1115 schemes in a global ocean circulation model at eddy-permitting resolu-  
1116 tion, *Ocean Dyn.*, *56*, 543–567.  
1117 Beuvier, J., F. Sevault, M. Herrmann, H. Kontoyiannis, W. Ludwig,  
1118 M. Rixen, E. Stanev, K. Béranger, and S. Somot (2010), Modeling the  
1119 Mediterranean Sea interannual variability during 1961–2000: Focus on  
1120 the Eastern Mediterranean Transient (EMT), *J. Geophys. Res.*, *115*,  
1121 C08017, doi:10.1029/2009JC005950.  
1122 Blanke, B., and P. Delecluse (1993), Variability of the tropical Atlantic  
1123 Ocean simulated by a general circulation model with two different mixed  
1124 layer physics, *J. Phys. Oceanogr.*, *23*, 1363–1388.  
1125 Bozec, A., P. Bouret-Aubertot, D. Iudicone, and M. Crépon (2008), Impact  
1126 of penetrative solar radiation on the diagnosis of water mass transforma-  
1127 tion in the Mediterranean Sea, *J. Geophys. Res.*, *113*, C06012,  
1128 doi:10.1029/2007JC004606.  
1129 Castellari, S., N. Pinardi, and K. Leaman (2000), Simulation of water mass  
1130 formation processes in the Mediterranean Sea: Influence of the time  
1131 frequency of the atmospheric forcing, *J. Geophys. Res.*, *105*(C10),  
1132 24,157–24,181, doi:10.1029/2000JC900055.  
1133 CLIPPER Project Team (1999), Modélisation à haute résolution de la cir-  
1134 culation dans l’océan Atlantique forcée et couplée océan-atmosphère,  
1135 *Sci. Tech. Rep. CLIPPER-R3-99*, Lab. des Ecoulements Géophys. et  
1136 Ind., Grenoble, France.  
1137 Déqué, M., and J. Pielikevire (1995), High-resolution climate simulation  
1138 over Europe, *Clim. Dyn.*, *11*, 321–339.  
1139 Font, J., P. Puig, J. Salat, A. Palanques, and M. Emelianov (2007),  
1140 Sequence of hydrographic changes in NW Mediterranean deep water  
1141 due to the exceptional winter of 2005, *Sci. Mar.*, *71*, 339–346.  
1142 García Lafuente, J., A. Sánchez Román, G. Díaz del Río, G. Sannino, and  
1143 J. C. Sánchez Garrido (2007), Recent observations of seasonal variability

of the Mediterranean outflow in the Strait of Gibraltar, *J. Geophys. Res.*, *114*  
1144 *112*, C10005, doi:10.1029/2006JC003992.  
1145 Gasparini, G., A. Ortona, G. Budillon, M. Astraldi, and E. Sansone (2005),  
1146 The effect of the Eastern Mediterranean Transient on the hydrographic  
1147 characteristics in the Strait of Sicily and in the Tyrrhenian Sea, *Deep*  
1148 *Sea Res., Part II*, *52*, 915–935.  
1149 Gibson, J., P. Kållberg, S. Uppala, A. Hernandez, and E. Serano (1997),  
1150 ERA description, in *Re-anal. Proj. Rep. Ser.*, Eur. Cent. for Medium-  
1151 Range Weather Forecast, Reading, U. K.  
1152 Guldberg, A., E. Kaas, M. Déqué, S. Yang, and S. Vester Thorsen (2005),  
1153 Reduction of systematic errors by empirical model correction: Impact on  
1154 seasonal prediction skill, *Tellus, Ser. A*, *57*, 575–588.  
1155 Herrmann, M. J., and S. Somot (2008), Relevance of ERA40 dynamical  
1156 downscaling for modeling deep convection in the Mediterranean Sea,  
1157 *Geophys. Res. Lett.*, *35*, L04607, doi:10.1029/2007GL032442.  
1158 Herrmann, M., S. Somot, F. Sevault, C. Estournel, and M. Déqué (2008),  
1159 Modeling the deep convection in the northwestern Mediterranean sea  
1160 using an eddy-permitting and an eddy-resolving model: Case study of  
1161 winter 1986–1987, *J. Geophys. Res.*, *113*, C04011, doi:10.1029/  
1162 2006JC003991.  
1163 Herrmann, M., J. Bouffard, and K. Béranger (2009), Monitoring open-  
1164 ocean deep convection from space, *Geophys. Res. Lett.*, *36*, L03606,  
1165 doi:10.1029/2008GL036422.  
1166 Kalnay, E., et al. (1996), The NCEP/NCAR 40-year reanalysis project,  
1167 *Bull. Am. Meteorol. Soc.*, *77*, 437–471.  
1168 López-Jurado, J.-L., C. González-Pola, and P. Vélaz-Belchí (2005), Obser-  
1169 vation of an abrupt disruption of the long-term warming trend at the  
1170 Balearic Sea, western Mediterranean Sea, in summer 2005, *Geophys.*  
1171 *Res. Lett.*, *32*, L24606, doi:10.1029/2005GRL024430.  
1172 Madec, G. (2008), NEMO ocean engine, *Note Pole de Modélisation 27*,  
1173 Inst. Pierre-Simon Laplace, Paris.  
1174 Marshall, J., and F. Schott (1999), Open-ocean convection: Observations,  
1175 theory, and models, *Rev. Geophys.*, *37*(1), 1–64.  
1176 MEDAR/MEDATLAS Group (2002), *MEDAR/MEDATLAS 2002 Data-*  
1177 *base: Cruise Inventory, Observed and Analysed Data of Temperature*  
1178 *and Bio-Chemical Parameters* [4 CD-ROMs], Inst. Fr. de Rech. Pour  
1179 l’Exploit. de la Mer, Brest, France.  
1180 Mertens, C., and F. Schott (1998), Interannual variability of deep-water  
1181 formation in the northwestern Mediterranean, *J. Phys. Oceanogr.*, *28*,  
1182 1410–1424.  
1183 Millot, C. (1999), Circulation in the western Mediterranean Sea, *J. Mar.*  
1184 *Syst.*, *20*, 423–442.  
1185 Millot, C. (2005), Circulation in the Mediterranean Sea: Evidences, debates  
1186 and unanswered questions, *Sci. Mar.*, *69* 5–21, doi:10.3989/scimar.  
1187 2005.69s15.  
1188 Perry, K. (2001), SeaWinds on QuikSCAT Level 3 Daily, Gridded Ocean  
1189 Wind Vectors (JPL SeaWinds Project), [http://podaac.jpl.nasa.gov/  
1190 DATA\\_CATALOG/quikscatinfo.html](http://podaac.jpl.nasa.gov/DATA_CATALOG/quikscatinfo.html), JPL Phys. Oceanogr. DAAC,  
1191 Pasadena, Calif.  
1192 Reynaud, T., P. Legrand, H. Mercier, and B. Barnier (1998), A new anal-  
1193 ysis of hydrographic data in the Atlantic and its application to an inverse  
1194 modeling study, *Int. World Ocean Circ. Exp. Newsl.* *32*, Natl. Oceanogr.  
1195 Data Cent., Silver Spring, Md.  
1196 Rixen, M., et al. (2005), The Eastern Mediterranean Deep Water: A proxy  
1197 for climat change, *Geophys. Res. Lett.*, *32*, L12608, doi:10.1029/  
1198 2005GL022702.  
1199 Roether, W., B. Klein, B. Manca, A. Theocharis, and S. Kioroglou (2007),  
1200 Transient eastern Mediterranean deep waters in response to the massive  
1201 dense-water output of the Aegean Sea in the 1990s, *Prog. Oceanogr.*, *74*,  
1202 540–571.  
1203 Salat, J., M. Emelianov, and J. López-Jurado (2006), Unusual extension of  
1204 western Mediterranean deep water formation during winter 2005, paper  
1205 presented at 5 Asamblea Hispano-Portuguesa de Geodesia y Geofísica,  
1206 Minist. de Medio Ambiente, Sevilla, Spain.  
1207 Sannino, G., M. Herrmann, A. Carillo, V. Rupolo, V. Ruggiero, V. Artale,  
1208 and P. Heimbach (2009), An eddy-permitting model of the Mediterr-  
1209 anean Sea with a two-way grid refinement at the Strait of Gibraltar, *Ocean*  
1210 *Modell.*, *30*, 56–72, doi:10.1016/j.ocemod.2009.06.002.  
1211 Schröder, K., G. P. Gasparini, M. Tangherlini, and M. Astraldi (2006),  
1212 Deep and intermediate water in the western Mediterranean under the  
1213 influence of the Eastern Mediterranean Transient, *Geophys. Res. Lett.*,  
1214 *33*, L21607, doi:10.1029/2006GL027121.  
1215 Schroeder, K., A. Ribotti, M. Borghini, R. Sorgente, A. Perilli, and  
1216 G. P. Gasparini (2008), An extensive Western Mediterranean Deep  
1217 Water renewal between 2004 and 2006, *Geophys. Res. Lett.*, *35*,  
1218 L18605, doi:10.1029/2008GL035146.  
1219 Schroeder, K., S. A. Josey, M. Herrmann, L. Grignon, G. P. Gasparini, and  
1220 H. L. Bryden (2010), Abrupt warming and salting of the Western Medi-

- 1222 iterranean Deep Water: Atmospheric forcings and lateral advection, 1237  
 1223 *J. Geophys. Res.*, *115*, C08029, doi:10.1029/2009JC005749. 1238  
 1224 Sevault, F., S. Somot, and J. Beuvier (2009), A regional version of the 1239  
 1225 NEMO ocean engine on the Mediterranean Sea: NEMOMED8 user's 1240  
 1226 guide, *Note Cent. 107*, Groupe de Météorol. de Grande Echelle et Climat, 1241  
 1227 CNRM, Toulouse, France. 1242  
 1228 Smith, R. O., H. L. Bryden, and K. Stansfield (2008), Observations of new 1243  
 1229 Western Mediterranean Deep Water formation using Argo floats 2004– 1244  
 1230 2006, *Ocean Sci.*, *4*, 133–149. 1245  
 1231 Smith, W., and D. Sandwell (1997), Global sea floor topography from sat-  
 1232 ellite altimetry and ship depth sounding, *Science*, *277*(5334), 1956–1962.  
 1233 Somot, S., F. Sevault, and M. Déqué (2006), Transient climate change sce-  
 1234 nario simulation of the Mediterranean Sea for the twenty-first century  
 1235 using a high-resolution ocean circulation model, *Clim. Dyn.*, *27*, 851–  
 1236 579, doi:10.1007/s00382-006-0167-z.
- Stanev, E., P.-Y. Le Traon, and E. Peneva (2000), Sea level variations and  
 their dependency on meteorological and hydrological forcing: Analysis  
 of altimeter and surface data for the Black Sea, *J. Geophys. Res.*,  
*105*(C7), 17,203–17,216.
- Testor, P., and J.-C. Gascard (2006), Post-convection spreading phase in  
 the northwestern Mediterranean Sea, *Deep Sea Res., Part I*, *53*, 869–893.
- Vörösmarty, C., B. Fekete, and B. Tucker (1996), *Global River Discharge  
 Database (RivDis)*, *Int. Hydrol. Program*, Global Hydrol. Archive and  
 Anal. Syst., UNESCO, Paris.
- J. Beuvier, ENSTA-ParisTech/UME, Chemin de la Hunière, F-91761  
 Palaiseau CEDEX, France. 1246  
 M. Herrmann, F. Sevault, and S. Somot, CNRM-GAME, Météo-France, 1247  
 42 Ave. Gaspard Coriolis, F-31057 Toulouse CEDEX, France. (marine. 1248  
 herrmann@m4x.org) 1249  
 1250

Article in Proof